

# GALEX Measurements of the Big Blue Bump in Soft X-ray Selected AGN

David W. Atlee

and

Smita Mathur

*Department of Astronomy, The Ohio State University*

atlee@astronomy.ohio-state.edu

## ABSTRACT

We study the UV properties of Type I AGN from the ROSAT All-Sky Survey that have been selected to show unusually soft X-ray continua. We examine a sample of 54 Seyfert 1 galaxies with detections in both Near-UV and Far-UV bands of the Galaxy Evolution Explorer (GALEX) satellite. Our sample is systematically fainter in the UV than galaxies studied in similar work by previous authors. We look for correlations between their UV and X-ray properties as well as correlations of these properties with either black hole mass or Eddington ratio. The shape of the Big Blue Bump (BBB) in the GALEX regime does not appear to correlate with its strength relative to the power law continuum, which conflicts with results reported by previous authors. The strength of the BBB is correlated with the shape of the X-ray continuum, in agreement with previous work, but the slope of the correlation is different than previously reported. The properties of the accretion disks of Type I AGN in the GALEX regime are relatively independent of black hole mass and Eddington ratio. We compare our measurements to the predictions of alternative theories for the origin of the soft excess, but we are unable to distinguish between Comptonization of BBB photons by a hot plasma and absorption in relativistic winds as the most likely origins for the soft X-ray excess.

*Subject headings:* galaxies: Seyfert, ultraviolet: general, X-ray: general

## 1. Introduction

The soft X-ray excess is a contribution to the 0.2-2 keV flux in some Type I AGN beyond that predicted by extrapolating the hard X-ray power-law. It was first reported by

Arnaud et al. (1985), who suggested that it was caused by thermal emission from the hot inner portion of the AGN accretion disk. Early observational work by Turner & Pounds (1989) using EXOSAT and subsequently by Walter & Fink (1993; WF93) using ROSAT further explored the properties of the soft excess in an attempt to conclusively determine its origin. Turner & Pounds (1989) found their results to be consistent with the soft excess arising from the high-energy tail of the thermal accretion disk emission for AGN, but WF93 found that their measurements using a combination of X-ray measurements from ROSAT and Ginga and UV fluxes from the International Ultraviolet Explorer (IUE) were inconsistent with simple thick or thin accretion disk models. They also discovered that the ROSAT spectral indices ( $\alpha_x$ ) of AGN with soft excesses were strongly correlated with the strength of the excess. The results of WF93 were later verified by Walter et al. (1994) using simultaneous IUE and ROSAT observations.

Several alternative theories for the origin of the soft excess have since been proposed. The current models tend to favor either reprocessing of thermal disk emission via Compton scattering in thermal plasmas (e.g. Kawaguchi, Shimura & Mineshige 2001, Niedźwiecki & Zdziarski 2006) or relativistically broadened absorption (e.g. Schurch & Done 2007). Models invoking atomic processes to generate the soft excess were originally proposed by Gierliński & Done (2004), who noted that the soft excess shows very consistent “temperature” across AGN with a wide variety of black hole masses. Schurch & Done (2006) recently proposed an alternative picture to the usual wind model for atomic origins. Their “failed” wind model does not require the massive outflow from the accretion disk usually required to make an atomic origin viable.

Several additional theories have also been proposed, including Compton reflection of hard X-ray photons by the dense, low-ionization gas in the accretion disk, resulting in an emergent spectrum that is very steep in the soft X-ray regime (Ross & Fabian 1993; Sobolewska & Done 2007; Done & Nayakshin 2007). Alternatively, hard X-ray photons could be absorbed by the disk instead of being reflected, and the absorbed energy would be re-emitted as soft X-ray photons with spectral indices that depend on the properties of the disk (Różańska et al. 2002). Another popular class of model is the slim disk model, originally proposed by Muchotrzeb & Paczyński (1982), in which super-Eddington accretion causes changes in the properties of the standard thin disk, causing it to become geometrically thick and optically thin in its inner region and emit high-energy photons (Chen & Wang 2004). For more recent theoretical treatments of slim disks, see e.g. Heinzeller, Mineshige & Ohsuga (2006) and Heinzeller & Duschl (2007).

After WF93, much of the observational work on the soft excess focused on the X-ray properties at the expense of the UV. The seminal paper from Boller, Brandt & Fink (1996),

which first reported the different distributions of  $\Gamma_x$  seen in Narrow-Line Seyfert 1 galaxies (NLS1s) and normal Seyfert 1 galaxies (BLS1s) is one example. However, it is often difficult to distinguish between the various competing models based only on goodness of fit to X-ray spectra (e.g. Sobolewska & Done 2007; Piro et al. 1997), and each of the competing models has its drawbacks. Comptonization models require nearly constant temperatures, and absorption models tend to produce sharper absorption lines than desirable, for example.

In Grupe et al. (1998, 2004; G98, G04), large samples of Seyfert 1 galaxies with strong soft excesses were drawn from the full set of optically-identified ROSAT All-Sky Survey (RASS) sources. Some of their conclusions were similar to those of WF93, but in neither paper did the authors examine the UV fluxes of their sample. Since the publication of WF93, a number of papers have examined the UV properties of a handful of soft excess AGN (Puchnarewicz et al. 1995a; Puchnarewicz et al. 1995b) and NLS1 galaxies (Kuraszkiewica et al. 2000; Leighly & Moore 2004). Other work has focused on large samples of AGN with data from multiple wavelength regimes (e.g. Strateva et al. 2005, Mainieri et al. 2007 Kelly et al. 2008), but there have been no attempts to study the UV properties of a moderately large, uniformly-selected sample of soft excess AGN.

The samples of G98 and G04 were selected to show unusually soft ROSAT spectra, so these AGN all show significant soft excesses. The samples were also selected uniformly in their X-ray properties, and they contain reasonably large numbers of objects. We use Galaxy Evolution Explorer (GALEX) fluxes to study the UV properties of these objects, determining the shape and relative strength of the Big Blue Bump (BBB). By measuring the BBB directly and relating its properties to the soft excess, we can provide additional constraints on the physical mechanism responsible for generating the soft X-ray excess. In §2 we discuss the observations we collected and the extraction of the necessary parameters. In §3 we discuss the analysis we perform on the extracted parameters, and in §4 we compare our results with the predictions of theories for the origin of the soft excess.

Luminosities in this paper are calculated using  $H_0 = 72 \text{ km s}^{-1}$ ,  $\Omega_m = 0.27$  and  $\Omega_\Lambda = 0.73$ .

## 2. AGN Sample

Grupe et al. (1998, 2004) selected samples of soft, X-ray bright AGN at high Galactic latitude from the RASS. They required that their objects all have ROSAT hardness ratios (HR) less than zero, yielding a sample of AGN with relatively strong soft excesses. We

acquired GALEX Release 3 (GR3)<sup>1</sup> images of the G98 and G04 AGN wherever possible. Measuring the Near-UV ( $NUV$ ,  $\lambda_{eff} = 2271\text{\AA}$ ) and Far-UV ( $FUV$ ,  $\lambda_{eff} = 1528\text{\AA}$ ) fluxes from the GR3 images, we constructed a sample of 54 AGN with measurements of both the UV and soft X-ray fluxes. These AGN are listed in Table 1.

We extracted X-ray count rates and spectral indices for the AGN in our sample from Grupe et al. (2001, 2004) wherever possible, and from Grupe et al. (1998, 1999) otherwise. Following the convention in these papers, we list X-ray spectral indices in energy units, i.e.  $F_\nu \propto \nu^{-\alpha_x}$ , where  $\alpha_x$  is measured in the ROSAT band (0.2-2.0 keV). This differs from the convention of WF93, who list photon indices ( $\Gamma_x = \alpha_x + 1$ , where  $N_\nu \propto \nu^{-\Gamma_x}$ ). We have accounted for this difference when comparing with their results. The spectral indices for galaxies in the Grupe et al. catalogs are higher than for the average AGN, as expected for a sample of soft excess AGNs, but our  $\langle\alpha_x\rangle$  is even higher than the average of the WF93 sample (2.1 compared to 1.5 in WF93). This shift in  $\langle\alpha_x\rangle$  is due primarily to the inclusion of a large Narrow-Line Seyfert 1 (NLS1) subsample, as NLS1s are known to exhibit softer X-ray continua (larger  $\alpha_x$ ; Boller, Brandt & Fink 1996).

Our AGN sample has only three objects (NGC 4593, Mrk 142 & 478) in common with the WF93 sample, despite covering roughly the same ranges in redshift and X-ray flux. This is due to selection effects, as WF93 required that their objects have UV (International Ultraviolet Explorer; IUE), 5 GHz radio continuum and hard X-ray (Ginga) flux measurements in addition to their ROSAT fluxes. We supplemented the information in the Grupe et al. catalogs with IRAS  $25\mu m$  fluxes from the NASA Extragalactic Database (NED<sup>2</sup>, various authors). We found  $25\mu m$  fluxes for only 17 of the 54 objects in our sample, so we use the IRAS fluxes only to verify that our primary strength indicator for the BBB is unbiased with respect to the strengths reported by WF93 (see Section 3.1).

The majority of the GALEX images available for our sample come from the GALEX All-Sky Imaging Survey (AIS), which have  $\sim 100$  s exposure per field. Two objects (Mrk 1048 and PG 1244+026) also had deeper Medium Imaging Survey exposures, and Markarian 1048 had another, still deeper, exposure from the Guest Investigator program. QSO 0056-36 also had a second AIS exposure. The GALEX exposure times associated with each object are listed in Table 1, along with several other important parameters including UV fluxes, X-ray count rates and  $H\beta$  line widths. We required that all objects in our sample have detections in both the  $NUV$  and  $FUV$ , but this restriction did not result in excluding any objects from our sample.

---

<sup>1</sup><http://galex.stsci.edu/GR3>

<sup>2</sup><http://nedwww.ipac.caltech.edu>

We divided our AGN into Narrow-Line Seyfert 1 (NLS1) and normal Seyfert 1 (BLS1) classes based on the width of the  $H\beta$  emission line. All objects with  $\text{FWHM}(H\beta) < 2000 \text{ km s}^{-1}$  were classified as NLS1s. We used the line widths listed in Grupe et al. (2004) wherever possible and widths from Grupe et al. (1999) otherwise, classifying 29 of our 54 AGN as NLS1s. Markarian 734, which is listed only in the Grupe et al. (1999) catalog, has  $\text{FWHM}(H\beta)$  and  $\alpha_x$  similar to four NLS1s that would be classified as BLS1s based on their Grupe et al. (1999) line widths (see Table 2). This suggests that the classification of Mrk 734 as a BLS1 may be erroneous. Removing it from the sample has no significant effect on our conclusions.

## 2.1. Flux Extraction

We measured GALEX  $FUV$  and  $NUV$  count rates within  $18''$  photometric apertures for each AGN in our sample. We converted the measured count rates to magnitudes using the GALEX photometric zero-points of Morrissey et al. (2005),

$$m_{FUV} = -2.5 \log(C_{FUV}) + 18.82 \quad (1)$$

$$m_{NUV} = -2.5 \log(C_{NUV}) + 20.08 \quad (2)$$

where  $C_x$  is the count rate in bandpass  $x$ . To compute the Galactic extinction corrections, we averaged the reddening law of Cardelli, Clayton & Mathis (1989) across the  $FUV$  and  $NUV$  effective area curves,

$$R_X = \frac{\int_{\lambda_1}^{\lambda_2} R(\lambda)T(\lambda)d\lambda}{\int_{\lambda_1}^{\lambda_2} T(\lambda)d\lambda}, \quad (3)$$

where  $R(\lambda)$  is the Cardelli, Clayton & Mathis (1989) R-value at wavelength  $\lambda$ , and  $T(\lambda)$  is the filter bandpass. We found  $R_{FUV} = 8.24$  and  $R_{NUV} = 8.10$ . The R-values and  $E(B - V)$  color excesses for each line of sight (Schlegel et al. 1998) were used to compute total extinction and correct the measured fluxes for each object. We used the AB-magnitude relation to convert the dereddened magnitudes to UV flux densities, and we used PIMMS to solve for  $F_\nu(2 \text{ keV})$  for our AGN using the X-ray count rates and spectral indices recorded in the Grupe catalogs. Grupe et al. fixed column densities at the Galactic value unless  $N_{H,fit} > N_{H,gal} + 2 \times 10^{20} \text{ cm}^{-2}$ , in which case the fitted value was used. Determining  $F_\nu$  in this way assumes that  $\alpha_x$  provides a good description of the X-ray spectrum across the entire ROSAT energy range. This assumption is not perfect and is likely to do worse in objects with steeper spectra, so some results may be biased. However, the number of objects with extremely steep spectra is limited (4 objects with  $\alpha_x > 3$ ), and the uncertainties on these indices are relatively large, so any biases in the measurements are covered by the error budget.

## 2.2. Black Hole Masses

We use black hole masses and Eddington ratios ( $L/L_{\text{edd}}$ ) from Grupe & Mathur (2004), which include 30 of our 54 AGNs. These black hole masses were determined using the Kaspi et al. (2000) relations, which was calibrated empirically using reverberation mapped AGNs. The calibration sample included several AGN with luminosities similar to the AGN in our sample, so the Kaspi relation should yield reasonably robust black hole masses. Bentz et al. (2006) reported a different scaling relation with a power law index of  $0.52 \pm 0.04$ , which is in agreement with the value expected from theory. If we use the Bentz relation instead of the Kaspi relation, we find significantly larger black hole masses than computed by Grupe & Mathur (2004), but this is not unexpected since the stellar continuum has not been subtracted from  $L_{5100 \text{ \AA}}$  for our AGN sample, resulting in an over-estimate of the radius of the Broad Line Region (BLR). The alternative masses have a significant impact on some of the measured correlations, which can be seen by comparing the correlation coefficients in Tables 3 and 4. Unsurprisingly, using the alternative  $L_{\lambda}(5100 \text{ \AA})-R_{\text{BLR}}$  relation has the largest impact on correlations with  $L_{\lambda}(5100 \text{ \AA})$ ; the other changes are rarely significant. Because we have no information on the host galaxies of our AGN, we have elected to use the empirically calibrated Kaspi relation. This will add scatter to our inferred black hole masses, but based on the few qualitative differences between Tables 3 and 4 we infer that the potential to introduce or hide correlations is limited.

We might also consider the impact of radiation pressure on the derived black hole masses, as described by Marconi et al. (2008). Qualitatively, the impact of radiation pressure should result in higher masses for systems radiating closer to their Eddington rate, and Marconi et al. (2008) found that, after applying this correction, the Eddington ratios of NLS1 systems are less extreme than result from applying the Bentz and Kaspi relations. Computing black hole masses using the Marconi relation rather than the Kaspi relation yields masses that are, on average, 0.2 dex larger. The new masses are correlated with the old masses with  $r_s = 0.69$ . However, Marconi et al. failed to account for the lower Eddington ratios and reduced radiation pressure implied by the adjusted black hole masses. As a result, their results overestimate black hole masses in systems where the corrections for radiation pressure are significant, and the difference between the “true” black hole masses and the results calculated using the Kaspi relation will be less than the 0.2 dex implied by applying the Marconi relation.

Netzer (2009) found that black hole masses determined using the Marconi relation are distributed differently from black hole masses in type 2 AGNs, suggesting that radiation pressure is not important in nearby AGNs. However, Marconi et al. (2009) in turn suggested that the differences found by Netzer (2009) can be attributed to scatter in the underlying

scaling relations rather than a lack of radiation pressure support in the BLR. Nevertheless, Marconi et al. (2009) and Netzer (2009) agree that the Marconi et al. (2008) relation is unable to successfully reproduce the “true,” underlying mass distribution, indicating that more work is needed. For the rest of this paper, we consider masses resulting from the Kaspi relation with the caveat that the systematic uncertainties associated with the alternative methods for calculating black hole mass must also be considered.

The masses resulting from applying the Kaspi relation are more properly called virial products, which differ from the true black hole mass by a geometric factor  $f$ . There is significant debate in the literature on the proper value of this constant. Using the dispersion of the  $H\beta$  emission line to measure the virial products, Onken et al. (2004) found that a statistical correction of  $f = 5.5$  was required to bring their virial masses into agreement with black hole masses predicted by the  $M_{BH} - \sigma_*$  relation. By contrast, Watson, Mathur & Grupe (2007) found a correction of  $f = 2.2$  for AGN in the Grupe et al. (2004) sample using the line dispersion or  $f = 0.55$  using FWHM. The latter value disagrees with the results of Kaspi et al. (2000), who found  $f = 0.75$ . Watson, Mathur & Grupe (2007) also found that there is a systematic difference between the geometric corrections required to bring the BLS1 and NLS1 samples into agreement with the  $M_{BH} - \sigma_*$  relation. Given this disagreement, we choose not to apply a geometric factor and simply use the virial products. As a result, the absolute masses and Eddington ratios we use are incorrect, but there will be little effect on the measured correlations as long as  $f$  is a constant. If the geometric corrections required by NLS1s and BLS1s do indeed differ, the impact of using virial products instead of actual black hole masses might be significant.

### 3. Correlation Analysis

In this section, we examine the differences in several measurable parameters between NLS1s and BLS1s. We also study the relationships between the parameters themselves. We examine several observables, including flux ratios and  $\alpha_x$ , as well as the physical characteristics ( $M_{BH}$ ,  $L/L_{\text{edd}}$  and  $L$ ) that determine the properties of each AGN. Walter & Fink (1993) found that the strength of the soft X-ray excess, measured using hard X-ray fluxes from Ginga and soft X-ray fluxes from ROSAT, correlates well with the ROSAT spectral index (WF93, Fig 7). Based on this result, they used  $\Gamma_x$  as a proxy for the strength of the soft excess. We take a similar approach, using  $\alpha_x$  instead of  $\Gamma_x$ , to examine the relationships between the soft X-ray excess and the UV properties of the AGN in our sample. However, it is important to note that when we discuss the “soft X-ray excess” below, we actually mean the shape of the soft X-ray continuum.

### 3.1. Observables

In Figure 1, we compare an indicator for the strength of the BBB with respect to the hard X-ray continuum  $\left(\nu F_\nu(1528 \text{ \AA})/\nu F_\nu(2 \text{ keV})\right)$  with  $\alpha_x$  to verify that the correlation between the strength of the BBB and the soft excess, as reported by WF93, also appears in our sample. We find a significant correlation in both the NLS1 and BLS1 samples as well as in the merged sample, as indicated in Table 5. It is apparent that the majority of the BLS1s lie on or near the WF93 relation, but the NLS1s are located systematically above the WF93 best-fit power law. Computing the best-fit relation to our data points in the figure yields

$$\alpha_x = (0.84 \pm 0.13) \log\left[\nu F_\nu(1528 \text{ \AA})/\nu F_\nu(2 \text{ keV})\right] + (0.85 \pm 0.15) \quad (4)$$

which is steeper than the WF93 best-fit, which has slope  $0.68 \pm 0.1$ . The two fits overlap in the regime occupied by the BLS1s, and the steeper slope of our fit is driven by the NLS1s in our sample. A two-dimensional KS test confirms that the NLS1 and BLS1 samples occupy a different region in the parameter space at the 99.5% confidence. Figure 2 shows that the NLS1 and BLS1 samples occupy similar ranges in bump strength, but the NLS1 sample shows extended tails at both ends.

We also computed the ratio  $\left(\nu F_\nu(2271 \text{ \AA})/\nu F_\nu(2 \text{ keV})\right)$  between the *NUV* and X-ray fluxes, which is analogous to  $\alpha_{\text{ox}}$ . The distributions of the flux ratio in both the NLS1 and BLS1 samples are shown in Figure 3. It is apparent that the NLS1 sample has more objects with high flux ratios, consistent with Figure 2, and a KS test indicates that the two distributions are different at about 97% confidence, which is suggestive but not especially significant. If we assume the UV continuum is well-described by a power-law, we can determine  $\alpha_{\text{ox}}$  for our AGNs by comparing the *FUV* and *NUV* fluxes. We find that the mean and median of the  $\alpha_{\text{ox}}$  distribution of the sample are both 1.4, consistent with the results of Elvis et al. (1994). However, we caution that this calculation requires extrapolating the UV power-law longward of the *NUV* effective wavelength, rendering  $\alpha_{\text{ox}}$  inherently less robust than the flux ratios shown in Figure 3. In either case, our AGNs appear to be quite typical in this respect, but there is marginal evidence that the NLS1s have slightly stronger BBB than usual, consistent with the results in Figure 1. If BBB photons are reprocessed to form the soft excess, a stronger BBB should be associated with a stronger soft excess, which indeed is observed. (In order to explain the flux ratios in Figure 1, only one in  $\sim 10^6$  BBB photons needs to be reprocessed. The associated UV flux decrement would not be observable.)

Many of our AGNs occupy the gap between the main locus of WF93 galaxies and their outliers, as shown in Figure 1, indicating a systematic difference between our AGNs and those of WF93. This difference could be caused either by weaker UV at fixed X-ray flux or by steeper  $\alpha_x$  at fixed BBB strength. It is apparent from Figure 4 that the X-ray spectra

of our galaxies are, on average, steeper than the galaxies of WF93 ( $\langle\alpha_x\rangle = 2.1$ , compared to  $\langle\alpha_x\rangle = 1.5$  for WF93). Comparing the far-UV and X-ray fluxes of our sample with the fluxes of the WF93 AGNs, we find that our AGNs are fainter in both the UV and X-ray, but the difference is larger in the UV. (The median is shifted by a factor of 5.7 in the UV, compared to 5.0 in the X-ray.) This, in combination with the higher average  $\alpha_x$  in our sample accounts for the observed differences between our sample and WF93’s. The difference between the median  $\nu F_\nu(1528 \text{ \AA})/\nu F_\nu(2 \text{ keV})$  in our sample and WF93’s might be attributable to their use of IUE observations to measure UV fluxes. The WF93 fluxes show a fractional error near unity for fluxes below  $\sim 3 \times 10^{-11}$ , whereas the typical GALEX uncertainty is only a few percent at these flux levels. We are therefore able to obtain significant GALEX detections of all of our sources, and our sample is unbiased with respect to UV flux.

While the majority of the BLS1s agree well with the WF93 best fit, the NLS1s are shifted systematically to higher  $\alpha_x$ . In combination with the good correlation between  $\nu F_\nu(1528 \text{ \AA})/\nu F_\nu(2 \text{ keV})$  and  $\alpha_x$  for the full sample, this indicates that the relation between the strength of the BBB and the shape of the soft X-ray continuum is steeper among AGN with the strongest soft excesses. This in turn suggests the need for a second parameter to account for the variation in  $\alpha_x$  at fixed BBB strength.

We identified 9 AGN that lie well away from the “main” relation between  $\nu F_\nu(1528 \text{ \AA})/\nu F_\nu(2 \text{ keV})$  and  $\alpha_x$ . These outliers are listed, along with a number of important properties, in Table 6. Five of the outliers show UV-optical luminosity ratios less than one, putting them well below the main locus in Figure 7. This suggests that the primary cause of our outliers is UV absorption. We fit a power law to the objects in Figure 7 with  $L_{FUV} \geq L_V$  and found,

$$\log(L_{FUV}/L_\odot) = 1.09 \log(L_V/L_\odot) - 0.65 \quad (5)$$

Assuming that all of the galaxies with  $L_{FUV} < L_V$  fall exactly on the best fit line, we require internal E(B-V) between 0.3 and 1.0 to explain the measured luminosity ratios. For the Galactic gas-to-dust ratio, this implies  $N_H \approx 5 \times 10^{21} \text{ cm}^{-2}$ , which is far larger than the column densities measured from X-ray spectral fits. We note, however, that the implied  $N_H$  is degenerate with  $\alpha_x$ , so these systems could have larger column densities and steeper spectra than reported, though this seems unlikely given the recorded values of  $\alpha_x$ . Also, WF93 found a small number of galaxies with significant internal extinction despite moderate column densities inferred from the ROSAT spectra of those systems. The unusual luminosity ratios shown in Figure 7 might also be an indication that the *FUV* and *V* band luminosities are dominated by young stars rather than by the AGN accretion disk. This hypothesis is supported by the unusually low values of  $\alpha_{ox}$  exhibited by three of these five objects. All three AGNs with such low  $\alpha_{ox}$  have  $L_{FUV} < 10^{43} \text{ erg s}^{-1}$ , which corresponds to a SFR of  $10 M_\odot \text{ yr}^{-1}$  (Salim et al. 2007).

Of the 4 outliers in Table 6 that do not appear to be strongly absorbed in Figure 7, 3 show unusually large  $\alpha_x$ , and the fourth (RX J0902-07) lies very close to the line dividing the “normal” AGNs from the outliers. This last object does not differ significantly from the “typical” AGNs in our sample for any of the parameters listed in Table 6, suggesting that it should be considered normal. The other outliers can be divided into two classes: objects that show UV absorption and objects that show extraordinarily high  $\alpha_x$ .

Most of our AGNs occupy the gap between the WF93 best-fit relation and their outliers. Walter & Fink (1993) explained their outliers as normal objects with strong intrinsic absorption, but few of our AGNs show evidence for UV absorption. Only 3 of the 8 objects with  $L_{FUV}/L_V < 1$  fall into our main sample, so strong UV absorption cannot be responsible for this difference between our sample and WF93’s. We note, however, that weak absorption is difficult to identify from Figure 7 due to the large intrinsic scatter about the mean relation, so weak intrinsic absorption might contribute to the shift in our sample away from the WF93 mean.

We also examine the relation between indicators for the strength of the BBB and its shape ( $\nu F_\nu(1528 \text{ \AA})/\nu F_\nu(2271 \text{ \AA})$ ), shown in Figure 8. Like WF93, we find a plateau accompanied by a sharp drop toward lower values of  $\nu F_\nu(1528 \text{ \AA})/\nu F_\nu(2 \text{ keV})$ . However, Figure 8 shows a broader scatter in the plateau region, plateaus at a lower ratio, and fills in the red tail of the distribution less completely than seen in the analogous diagram in WF93. Also, the objects occupying the “tail” of the distribution in Figure 8 are all listed as outliers in Table 6, which immediately suggests that the tail in our sample is due to absorption. The correlation between the strength and shape of the BBB disappears if we disregard the outliers, indicating that the shape of the BBB is largely independent of its strength.

The absence of any correlation between the shape and strength of the BBB is a direct contradiction of the results of WF93. We use very different methods to measure the shape parameter of the BBB, so it is possible that the disparity between our results and theirs are due to systematic biases, particularly since our wavelength baseline is only half theirs. However, the average UV flux ratio in Figure 8 ( $\langle \nu F_\nu(1528 \text{ \AA})/\nu F_\nu(2271 \text{ \AA}) \rangle \approx 1.4$ ) implies a power-law continuum ( $F_\nu \propto \nu^{-\alpha_{uv}}$ ) with  $\langle \alpha_{uv} \rangle \approx -0.85$ , which in turn suggests that  $\langle \nu F_\nu(1375 \text{ \AA})/\nu F_\nu(2675 \text{ \AA}) \rangle \approx 1.75$ . This is consistent with the plateau seen in WF93 Figure 11, which is at approximately 1.8. Given this agreement and the fact that the tail of our distribution is populated by AGNs showing probable absorption, we suggest that WF93 were too quick to dismiss absorption as a potential cause of their correlation.

To verify that the differences between Figure 8 and WF93’s Figure 11 are not caused by systematic differences between  $\nu F_\nu(1528 \text{ \AA})/\nu F_\nu(2 \text{ keV})$  and  $\nu F_\nu(1528 \text{ \AA})/\nu F_\nu(25 \mu m)$ , we

compare the two strength indicators in Figure 9. Despite the differences between the UV fluxes of the two samples, our galaxies show good agreement with the WF93 best-fit relation. We derive a best fit relation for our sample, obtaining

$$\frac{\nu F_\nu(1528 \text{ \AA})}{\nu F_\nu(25 \text{ \mu m})} = (0.95 \pm 0.08) \frac{\nu F_\nu(1528 \text{ \AA})}{\nu F_\nu(2 \text{ keV})} - (1.16 \pm 0.09) \quad (6)$$

which is consistent with the WF93 best fit within the uncertainties. Thus, there is no inherent bias in  $\nu F_\nu(1528 \text{ \AA})/\nu F_\nu(2 \text{ keV})$  compared to  $\nu F_\nu(1528 \text{ \AA})/\nu F_\nu(25 \text{ \mu m})$ , and the absence of a correlation between the shape and strength of the BBB among our AGN sample is not caused by differences between our strength indicator and WF93’s. It also indicates that the steeper relation between  $\alpha_x$  and  $\nu F_\nu(1528 \text{ \AA})/\nu F_\nu(2 \text{ keV})$  among our AGN compared to the WF93 sample is not due to systematic errors. This lends credence to the hypothesis that a factor besides the strength of the BBB must contribute to the shape of the soft X-ray continuum.

The structure of a standard thin disk, which might be reflected in the UV color of the disk, can depend on both black hole mass and Eddington ratio (see Eq. 8), so We want to know whether  $\nu F_\nu(1528 \text{ \AA})/\nu F_\nu(2271 \text{ \AA})$  shows systematic differences between the NLS1 and BLS1 samples. A KS test reveals that the distributions differ between the NLS1 and BLS1 samples at about 95% confidence, but this difference disappears when we eliminate the outliers (Tab. 6). Thus, we measure no intrinsic variation in the structure of accretion disks powering NLS1 and BLS1 AGNs. However, the GALEX bands are sensitive only to variations in disk structure if the Eddington ratio is well below  $\dot{m}$ . (See Figure 10.) As a result, we expect little intrinsic difference between the BLS1 and NLS1 AGN samples.

Finally, we look for any relationships of the indicators we have already examined with  $\text{FWHM}(\text{H}\beta)$ , which might tend to indicate systematic differences between the two classes of AGN. We find two trends that might be of interest: a correlation with  $\alpha_x$  among the merged AGN sample at  $> 99.9\%$  confidence and another with  $\nu F_\nu(1528 \text{ \AA})/\nu F_\nu(2271 \text{ \AA})$  among the NLS1 sample at 97% confidence. The second is interesting if true, because it would suggest that the structure of the BLR is related to the UV color of the accretion disk, but the correlation is not strong enough to support such a claim unequivocally. Figure 11 shows the relation between  $\text{FWHM}(\text{H}\beta)$  and  $\alpha_x$  and is consistent with the “zone of avoidance,” in which BLS1s generally have  $\alpha_x \lesssim 2.0$ , as reported by Boller, Brandt & Fink (1996). The measured correlation is a result of this effect.

### 3.2. Physical Parameters

We also examined the relationships between the observables discussed above and the physical parameters ( $M_{BH}$ ,  $\dot{m} = L/L_{\text{edd}}$  and  $L_{\text{bol}}$ ) that characterize each AGN, where the Eddington ratios were all determined using  $L_{\text{bol}}$  from the Grupe et al. catalogs. We find strong correlations ( $> 99\%$  confidence) of shape, strength and  $\alpha_x$  with UV luminosity among the NLS1 sample, as shown in Figure 12. We also find correlations of both strength and shape with luminosity in the merged sample, but the lack of correlation of  $\alpha_x$  with luminosity among BLS1s dilutes the correlation in the merged sample to 98% confidence. This is significantly weaker than the same correlation reported by Kelly et al. (2008) for a sample of optically-selected, radio-quiet quasars. This suggests that the shape of the X-ray continuum is more tightly coupled to the Big Blue Bump among optically selected AGN than among X-ray selected AGN. The Spearman correlation coefficients and significance values for the various parameters we examined are listed in Table 4.

The strong positive correlation of  $\nu F_\nu(1528 \text{ \AA})/\nu F_\nu(2271 \text{ \AA})$  with  $\nu L_\nu(1528 \text{ \AA})$  is in conflict with the results of Scott et al. (2004), who reported that the BBB, as measured in the FUSE band (900-1200  $\text{\AA}$ ) becomes softer in more luminous AGN. However, the GALEX *FUV* band does not overlap with the FUSE coverage, so the different variations with luminosity might be strictly a wavelength effect. If this is the case, the peak of the BBB in the average Seyfert AGN must lie somewhere between 1500 $\text{\AA}$  and 900 $\text{\AA}$ . The observed correlations are weaker but still significant ( $> 99\%$  confidence) if we consider  $\nu L_\nu(5100 \text{ \AA})$ . In Figures 12a and 12b, the relations exhibited by the NLS1 and BLS1 show good agreement, which is consistent with the structure of the accretion disks showing little variation between the two classes. We see very different relations of  $\alpha_x$  with luminosity between the NLS1 and BLS1 samples. This could be caused by most NLS1s being within a factor of a few in  $M_{BH}$ , causing variations in  $\dot{m}$  to drive a correlation of  $\alpha_x$  with luminosity.

From simple virial considerations, we expect that the width of the  $H\beta$  emission line should correlate with both  $M_{BH}$  and  $\dot{m}$ . If we assume the simplest possible relation,  $R_{BLR} \propto L^{1/2}$ , which is consistent with the results of Bentz et al. (2006), we find that  $w(H\beta) \propto (M_{BH}/\dot{m})^{1/4}$ . Examining the correlations in Table 4, we find that the  $H\beta$  line width is indeed correlated with both  $M_{BH}$  and  $\dot{m}$ , but the correlation is much stronger with  $M_{BH}/\dot{m}$ . Fitting the FWHM to  $M_{BH}/\dot{m}$  yields

$$\log \left[ w(H\beta) \right] = (0.24 \pm 0.01) \log(M_{BH}/\dot{m}) + (1.5 \pm 0.1) \quad (7)$$

with  $\chi_\nu^2 = 1.02$ , which is consistent with the simple prediction above. This relationship is also consistent with the results of McHardy et al. (2006), who found that the break timescale of the power density spectrum, which is proportional to  $M_{BH}/\dot{m}$ , is well correlated with line

width. This good agreement both with theory and with previous observations suggests that the Grupe & Mathur (2004) mass measurements are, on average, robust.

Our correlation measurements also agree with Piconcelli et al. (2005), who found a strong anti-correlation of  $\Gamma_{\text{soft}}$  with  $H\beta$  line width ( $r_s = -0.54$ ), where  $N_\nu \propto \nu^{-\Gamma_{\text{soft}}}$  is measured from 0.3–2.0 keV. In fact, the strength of the correlation they report is very similar to the strength of the correlation we find between FWHM and  $\alpha_x$  (our  $r_s = -0.53$ ), suggesting that much of the scatter between the two variables may be intrinsic. The errors on the line widths of NLS1s are comparable to the errors on BLS1 widths, so the lack of correlations with  $M_{BH}$  or  $\dot{m}$  among the BLS1 sample suggests that the geometry factor  $f$  varies more among the BLS1 sample than the NLS1 sample. This might happen if the BLR becomes more spherically symmetric at high Eddington ratio.

There is also a correlation of moderate significance (98.4% confidence) between  $M_{BH}$  and  $\nu F_\nu(1528 \text{ \AA})/\nu F_\nu(2271 \text{ \AA})$ , but correlation is positive, which is in opposition to the trend predicted for a standard thin disk (see Fig. 10). This correlation is probably spurious, since it is driven by a small number of AGNs with  $\nu F_\nu(1528 \text{ \AA})/\nu F_\nu(2271 \text{ \AA}) < 1$ , three of which are outliers in Figure 1. Two additional AGNs with  $\nu F_\nu(1528 \text{ \AA})/\nu F_\nu(2271 \text{ \AA}) < 1$  have  $L_{FUV} < \lambda L_\lambda(5100 \text{ \AA})$ , suggesting that low levels of recent star formation could significantly influence the measured UV flux ratio. After excluding both of these groups, we find no significant correlation of  $\nu F_\nu(1528 \text{ \AA})/\nu F_\nu(2271 \text{ \AA})$  with  $M_{BH}$ . There is no correlation of  $\nu F_\nu(1528 \text{ \AA})/\nu F_\nu(2271 \text{ \AA})$  with  $\dot{m}$  regardless of whether the AGNs with  $\nu F_\nu(1528 \text{ \AA})/\nu F_\nu(2271 \text{ \AA}) < 1$  are considered, which is expected given the relatively high Eddington ratios typical of the AGNs in our sample.

#### 4. Theoretical Models

We would like to use the UV properties of the observed AGNs to place constraints on theoretical models for the soft X-ray excess. We therefore compare the UV properties of our sample to predictions from various models. For the standard Shakura-Sunyaev thin disk, the temperature at the inner edge of the disk is given by their Eq. 3.8,

$$T_{\text{inner}} = 5 \times 10^8 \text{K} \alpha^{1/5} \dot{m}^{4/5} m^{-1/5} r_{ls}^{-3/2} \left(1 - r_{ls}^{-1/2}\right)^{4/5} \quad (8)$$

where  $m = M/M_\odot$  and  $r_{ls}$  is the last stable radius in units of the Schwarzschild radius. We computed  $T_{\text{inner}}$  for all the AGNs displayed in Figure 10, assuming  $\alpha = 0.1$ ,  $r_{ls} = 1.5$  and  $\dot{m}$  determined by the measured luminosities and black hole masses. We found that only NGC 7214 has a maximum disk temperature near  $(1+z)T_{FUV}$ . We note that NGC 7214 falls in the “main relation” in Figure 10 and has  $\nu F_\nu(1528 \text{ \AA})/\nu F_\nu(2271 \text{ \AA}) > 1$ , meaning

it is essentially normal. This is consistent with our argument that GALEX is insensitive to changes in the structure of the accretion disk. The accretion rates implied by the UV colors of our AGNs (Fig. 10) are substantially lower than the accretion rates determined using the bolometric luminosities from the literature ( $\dot{m} \gtrsim 0.1$ ). This implies that either the measured UV fluxes suffer from substantial intrinsic extinction, which would naturally redden the emergent spectrum, or the *NUV* fluxes might contain a substantial contribution from sources other than the accretion disk. Walter & Fink (1993) are able to measure the Balmer decrements for their sources, and they find that most of their sample suffers from little to no intrinsic extinction. Given the excellent agreement between the UV and MIR properties of their sample and ours (Figure 9), intrinsic extinction is highly unlikely to influence our results. The most likely source of a significant contribution to the *NUV* fluxes of our objects is low-level star formation, but a non-standard disk structure is also possible.

A popular class of models for non-standard accretion disks is the slim disk model first proposed by Muchotrzeb & Paczyński (1982), in which super-Eddington accretion drives the disk to puff up and change its structure. The super-Eddington accretion rates observed in several of our AGN suggest that this model might be applicable. Even more objects move into the slim disk regime if we consider the “corrected” black hole masses rather than the virial products, because the geometric factor for masses determined using the FWHM of the  $H\beta$  emission line is less than 1 (e.g. Watson, Mathur & Grupe 2007). The slim disk models of Wang & Netzer (2003) predict that the SED of the BBB rises steeply toward higher energy in the UV for even moderately super-Eddington accretion ( $\dot{m} \gtrsim 5$ ), so  $\nu F_\nu(1528 \text{ \AA})/\nu F_\nu(2271 \text{ \AA})$  should be greater than 1. This is generally true for our sample, but it is unable to explain the most unusual objects in Figure 10, which have UV flux ratios lying below rather than above the predictions of a standard thin disk. Furthermore, the slim disk model predicts that  $\alpha_x$  should decrease slightly with increasing  $\dot{m}$ , which has already been demonstrated to be false (e.g. Grupe 2004). Alternative slim disk models from Kawaguchi (2003) and Chen & Wang (2004) show similar failings. Furthermore, two of the most extreme objects in Figure 10 are BLS1s and show moderate Eddington ratios ( $\dot{m} = 0.08, 0.06$  respectively). This precludes the application of slim disk theory to these objects.

Models that rely on Comptonization of thermal photons in a hot plasma (e.g. Kawaguchi, Shimura & M 2001) are motivated by the strong correlation between  $\nu F_\nu(1375 \text{ \AA})/\nu F_\nu(2 \text{ keV})$  and  $\alpha_x$  reported by WF93. Because our sample differs systematically from the WF93 best-fit, we infer that an additional parameter related to the strength of the soft excess may influence the  $\nu F_\nu(1528 \text{ \AA})/\nu F_\nu(2 \text{ keV})-\alpha_x$  relation. However, the underlying model is supported by the strong correlation between the strength of the BBB and the shape of the soft X-ray continuum in our data. Given the significantly different  $\langle M_{BH} \rangle$  and  $\langle \dot{m} \rangle$  exhibited by BLS1s

and NLS1s, it is logical to infer that the temperature or density of the disk corona might be responsible for the different  $\nu F_\nu(1528 \text{ \AA})/\nu F_\nu(2 \text{ keV})-\alpha_x$  relations exhibited by the two samples, since both  $M_{BH}$  and  $\dot{m}$  can influence the structure of the corona. Since the BLS1s, on average, agree well with the WF93 results, this could also explain the differences between our merged sample and WF93’s results.

Models that suggest an atomic origin for the soft excess, originally proposed by Gierliński & Done (2004), postulate that the soft excess is actually a “hard deficit,” in which the X-ray flux in the range  $0.7 \text{ keV} \lesssim E \lesssim 5 \text{ keV}$  is subject to significant absorption by relativistically broadened OVII and OVIII lines. In a recent paper, Schurch & Done (2007) modeled the emergent X-ray spectrum that would be observed following absorption by material in a UV line-driven wind. They exclude this model based on sharp absorption features that appear in the model spectra but not in the spectra of real AGN. They also suggest that this could be resolved by invoking magnetically-driven outflow, which can potentially reach much larger terminal velocities.

Schurch & Done (2006) modeled the X-ray spectrum of PG 1211+143 with absorption in a high-velocity wind without subjecting the wind to any physical constraints. We want to determine whether our UV flux measurements are consistent with a smeared absorption model, assuming a mechanism to drive an outflow with the necessary velocity profile could be found. Since the X-ray continua in soft excess AGNs are generally smooth (Schurch & Done 2007), we assume that the multiplicative flux decrement from an input power-law continuum to the measured flux at 2 keV is linearly proportional to the strength of the soft X-ray excess. To relate the strength of the soft excess to the soft X-ray spectral index ( $\alpha_x$ ), we fit the soft excess and  $\Gamma_x$  measurements of by WF93, finding

$$\log(\Gamma_x) = (1.5 \pm 0.2) \log(X) + (1.9 \pm 0.1) \quad (9)$$

with  $\chi_\nu^2 = 0.59$ , where  $\Gamma_x$  is the photon spectral index in the ROSAT band, and  $X$  is the strength of the soft excess relative to the hard X-ray continuum, following WF93. Inverting this equation and transforming to  $\alpha_x$  yields:

$$\log(X) = \frac{\alpha_x - 0.9}{1.5} \quad (10)$$

We predict the flux decrements required to produce the measured  $\alpha_x$  in each of our sources using Equations 9 and 10 in combination with the rest-frame 2 keV flux decrement for PG 1211+143 required by Schurch & Done (2006;  $\alpha_{\text{cont}} = 1.37$ , flux decrement = 1.3 from their Figure 5).

To determine the minimum  $\nu F_\nu(1528 \text{ \AA})/\nu F_\nu(2 \text{ keV})$  required by the model, we need to know the shape of the input continuum for each AGN in our sample. We compute the

rest-frame  $F_\nu(5100 \text{ \AA})$  for each of our AGNs from the published  $L_\nu(5100 \text{ \AA})$  in Grupe et al. (1998, 2004), using measured  $F_\nu(2271 \text{ \AA})$  to estimate K-corrections and assuming a power-law continuum. We calculate the continuum shape ( $\alpha_{\text{cont}}$ ) from the measured 5100  $\text{\AA}$  and 2 keV fluxes for each of our AGNs,

$$\alpha_{\text{cont}} = -0.343 \left( \log[F_\nu(2 \text{ keV})] - \log[F_\nu(5100 \text{ \AA})] \right) \quad (11)$$

where the  $F_\nu$  are rest-frame fluxes, and the X-ray flux has been corrected for the appropriate flux decrement. Using  $\alpha_{\text{cont}}$  and the flux decrements required by our *ad hoc* model, we predict lower limits on  $\nu F_\nu(1528 \text{ \AA})/\nu F_\nu(2 \text{ keV})$  for each AGN.

We show the lower limits and measured flux ratios for our objects, excluding the outliers, in Figure 14. The blue triangles mark the six objects (H0439-27, Mrk 141, MCG+08-23-067, RX J1319+52, NGC 7214, RX J2349-31) whose lower limits exceed the measured flux ratios. The cumulative deficit distribution of these objects, normalized to the uncertainties in their flux ratios, is shown in Figure 15. This distribution is consistent with all of the objects having flux ratios intrinsically equal to the lower limits but scattered low by the observational errors. Thus, we cannot rule out an origin of the soft excess in smeared absorption based on our GALEX measurements.

While the AGNs in our sample are inconsistent with slim disk models, our measured flux ratios are consistent with either smeared absorption or Comptonization in a hot corona. We are therefore unable to favor either of these competing models, though the differences between our best-fit  $\nu F_\nu(1528 \text{ \AA})/\nu F_\nu(2 \text{ keV})$ — $\alpha_x$  relation and WF93’s indicates the need for a second parameter in the Comptonization model. We suggest this parameter might be the Eddington ratio.

## 5. Summary & Conclusions

We measure the UV fluxes of a sample of X-ray selected AGNs with strong soft X-ray excesses. We find that our AGNs are slightly fainter in the UV compared to the X-ray than a similar sample studied by WF93, and we conclude that these differences are attributable to selection effects.

We examine the relationships between several observables and the inferred physical properties of our AGN. We find that the shape of the soft X-ray continuum shows significant correlations with  $\nu F_\nu(1528 \text{ \AA})/\nu F_\nu(2 \text{ keV})$ , but the slope of the relation is steeper than that measured by WF93. This difference appears to result from selection effects. We conclude that the X-ray spectra of AGN with unusually steep soft X-ray continua, which belong to the

NLS1 class, are related to their UV spectra in a way fundamentally similar to AGN with more mundane soft X-ray spectra. The mechanism that drives the  $\nu F_\nu(1528 \text{ \AA})/\nu F_\nu(2 \text{ keV})-\alpha_x$  correlation must also lead to steeper  $\alpha_x$  at fixed  $\nu F_\nu(1528 \text{ \AA})/\nu F_\nu(2 \text{ keV})$  among NLS1s. The Eddington ratio might make a good choice for this second parameter, since the differences between our results and WF93’s are largest for the NLS1 sample.

We find a positive correlation of moderate significance between  $M_{BH}$  with the shape of the UV continuum, but this correlation disappears if we disregard objects lying far from in main locus in  $\nu F_\nu(1528 \text{ \AA})/\nu F_\nu(2 \text{ keV})-\alpha_x$  space. We also find no evidence for a correlation of  $\nu F_\nu(1528 \text{ \AA})/\nu F_\nu(2271 \text{ \AA})$  with  $L/L_{\text{edd}}$ . If the soft X-ray excess is caused by Comptonization of BBB photons in the hot corona of the accretion disk, a second parameter is needed to explain the large intrinsic variation in  $\alpha_x$  at fixed BBB strength. Because  $\alpha_x$  is known to depend strongly on  $L/L_{\text{edd}}$  while and the properties of the accretion disk vary only weakly with accretion rate,  $L/L_{\text{edd}}$  is the most obvious candidate.

We find no significant correlation between the color and strength of the BBB, so either the luminosity of the accretion disk relative to the underlying power law is independent of the temperature of the disk, or the characteristic temperature of the typical Seyfert 1 galaxy is outside the range where GALEX colors are sensitive ( $5\text{eV} \lesssim kT \lesssim 10\text{eV}$ ). The latter hypothesis is more likely based on the limited predicted range in GALEX colors for the black hole masses and accretion rates appropriate for our sample. Comparisons between predicted and measured flux ratios also suggest that the GALEX fluxes include contamination from young stars, obscuring any underlying correlation in objects with  $\nu L_\nu(1528\text{\AA}) \lesssim 5 \times 10^{43} \text{erg s}^{-1}$  (estimated SFR  $\lesssim 10 M_\odot \text{ yr}^{-1}$ ; Salim et al. 2007). Among our sample, there are 7(3) of 54(45) AGN in this luminosity range including (excluding) the outliers, so the impact of UV emission from young stars on our main conclusions will be small. Resolving the question of whether or not the shape and strength of the BBB are independent will likely require UV spectroscopy from HST, which has the resolution to separate host starlight from AGN emission and can be used to correct the measured flux ratios for redshift.

Finally, we are unable to use the UV fluxes of the Grupe et al. AGNs to distinguish between the absorption and Comptonization models for the origin of the soft X-ray excess. Resolving this question could have important implications for our understanding of AGN feedback, but the *ad hoc* model we use to estimate minimum  $\nu F_\nu(1528 \text{ \AA})/\nu F_\nu(2 \text{ keV})$  ratios does not provide sufficient predictive power to determine whether the absorption model really agrees with the UV flux measurements. Further study with a more detailed model is needed.

We thank an anonymous referee for insightful and penetrating comments which have significantly improved this paper. We are also grateful to G.C. Dewangan for helpful com-

ments and to Dirk Grupe for illuminating discussion regarding the ROSAT spectra used to construct his AGN samples. We also wish to thank the GALEX collaboration and the Space Telescope Science Institute for providing access to the UV images used in this work. GALEX is a NASA Small Explorer Class mission.

## REFERENCES

- Arnaud, M.A., et al. 1985, MNRAS, 217, 105
- Bentz, M., Peterson, B.M., Pogge, R.W., Vestergaard, M., & Onken, C.A. 2006, ApJ, 644, 133
- Boller, Th., Brandt, W.N. & Fink, H. 1996, A&A, 305, 53
- Cardelli, J.A., Clayton G.C., & Mathis, J.S. 1989, ApJ, 345, 245
- Chen, L. & Wang, J. 2040, ApJ, 614, 101
- Czerny, B. & Elvis, M. 1987, ApJ, 321, 305
- Czerny, B. et al. 2003, A&A, 412, 317
- Denney, K. D., et al. 2009, arXiv:0904.0251
- Dewangan, G.C., Griffiths, R.C., Dasgupta, S. & Rao, A.R. 2007, ApJ, 671, 1284
- Dickey, J.M. & Lockman, F.J. 1990, ARA&A, 28, 215
- Done, C., & Nayakshin, S. 2007, MNRAS, 377, L59
- Elvis, M. et al. 1994, ApJS, 95, 1
- Gierliński, M. & Done, C. 2004, MNRAS, 349, 7
- Gierliński, M. & Done, C. 2006, MNRAS, 371, 16
- Grupe, D., Beuermann, K., Thomas, H.-C., Mannheim, K., and Fink, H.H. 1998, A&A, 330, 25
- Grupe, D., Beuermann, K., Mannheim, K., and Thomas, H.-C. 1999, A&A, 350, 805
- Grupe, D., Thomas, H.-C. & Beuermann, K. 2001, A&A, 367, 470
- Grupe, D. 2004, ApJ, 127, 1799

- Grupe, D. & Mathur, S. 2004, *ApJ*, 606, L41
- Grupe, D., Wills, B.J., Leighly, K.M. & Meusinger, H. 2004, *ApJ*, 127, 156
- Heinzeller, D., Mineshige, S. & Ohsuga, K. 2006, *MNRAS*, 372, 1208
- Heinzeller, D. & Duschl, W.J. 2007, *MNRAS*, 374, 1146
- Kaspi, S., et al. 2000, *ApJ*, 533, 631
- Kawaguchi, T., Shimura, T. & Mineshige, S. 2001, *ApJ*, 546, 966
- Kawaguchi, T. 2003, *ApJ*, 593, 69
- Kelly, B. C., Bechtold, J., Trump, J. R., Vestergaard, M., & Siemiginowska, A. 2008, *ApJS*, 176, 355
- Kuraszkiewicz, J., Wilkes, B.J., Czerny, B. & Mathur, S. 2000, *ApJ*, 542, 692
- Laor, A. & Netzer, H. 1989, *MNRAS*, 238, 897
- Laor, A., Fiore, F., Elvis, M., Wilkes, B.J., McDowell, J.C. 1994, *ApJ*, 435, 611
- Leighly, K.M. & Moore, J.R. 2004, *ApJ*, 611, 107
- Mainieri, V., et al. 2007, *ApJ*, 172, 368
- Mannheim, K., Schulte, M. & Rachen, J. 1995, *A&A*, 303, L41
- Marconi, A., Axon, D. J., Maiolino, R., Nagao, T., Pastorini, G., Pietrini, P., Robinson, A., & Torricelli, G. 2008, *ApJ*, 678, 693
- Marconi, A., Axon, D., Maiolino, R., Nagao, T., Pietrini, P., Risaliti, G., Robinson, A., & Torricelli, G. 2009, arXiv:0905.0539
- McHardy, I.M., Koerding, E., Knigge, C., Uttley, P. & Fender, R.P. 2006, *Nature*, 444, L730
- Morrissey, P., et al. 2005, *ApJ*, 619, 7
- Muchotrzeb, B. & Paczyński, B. 1982, *Acta Astron.*, 32, 1
- Netzer, H. 2009, *ApJ*, 695, 793
- Niedźwiecki, A., & Zdziarski, A. A. 2006, *MNRAS*, 365, 606
- Onken, C.A., et al. 2004, *ApJ*, 615, 645

- Peterson, B.M., et al. 2000, 542, 161
- Piconcelli, E., Jimenez-Bailón, E., Guainazzi, M., Schartel, N., Rodríguez-Pascual, P.M., Santos-Lleó, M. 2005, A&A, 432, 15
- Piro, L., Matt, G., & Ricci, R. 1997, A&AS, 126, 525
- Pounds, K.A., Done, C. & Osborne, J.P. 1995, MNRAS, 277, L5
- Puchnarewicz, E.M., Mason, K.O., Siemiginowska, A. & Pounds, K.A. 1995, MNRAS, 276, 20
- Puchnarewicz, E.M., Granduardi-Raymont, G., Mason, K.O. & Sekiguchi, K. 1995, MNRAS, 276, 1281
- Ross, R.R. & Fabian, A.C. 1993, MNRAS, 261, 74
- Różańska, A., Dumont, A.-M., Czerny, B., & Collin, S. 2002, MNRAS, 332, 799
- Salim, S. et al. 2007, ApJS, 173, 267
- Schlegel, D.J., Finkbeiner, D.P. & Davis, M. 1998, ApJ, 500, 525
- Schurch, N.J. & Done, C. 2006, MNRAS, 371, 81
- Schurch, N.J. & Done, C. 2007, MNRAS, 381, 1413
- Scott, J.E. et al. 2004, ApJ, 615, 135
- Shakura, N.I. & Sunyaev, R.A. 1973, A&A, 24, 337
- Sobolewska, M. A., & Done, C. 2007, MNRAS, 374, 150
- Strateva, I.V., Brandt, W.N., Schneider, D.P., Vanden Berk, D.G. & Vignali, C. 2005, ApJ, 130, 387
- Turner, T.J. & Pounds, K.A. 1989, MNRAS, 240, 833
- Walter, R. & Fink, H.H. 1993, A&A, 274, 105
- Walter, R., et al. 1994, A&A, 285, 119
- Wang, J.-M. & Netzer, H. 2003, A&A, 398, 927
- Watson, L.C., Mathur, S. & Grupe, D. 2007, ApJ, 133, 2435

Table 1. Seyfert 1 Galaxy Sample

Name	$\alpha_{2000}$	$\delta_{2000}$	$z$	$N_{\text{H}}$ [ $10^{20}\text{cm}^{-2}$ ]	$\alpha_{\text{x}}$	$E(B - V)$	FWHM( $H\beta$ ) [ $\text{km s}^{-1}$ ]	$\nu F_{\nu}(1582 \text{ \AA})$ [ $10^{-12}\text{erg s}^{-1} \text{cm}^{-2}$ ]	$\nu F_{\nu}(2271 \text{ \AA})$ [ $10^{-12}\text{erg s}^{-1} \text{cm}^{-2}$ ]	$F_{\nu}(2 \text{ keV})$ [ $10^{-13}\text{erg s}^{-1} \text{cm}^{-2} \text{keV}^{-1}$ ]
RX J0022-34	00:22:33.0	-34:07:22	0.219	1.39	$1.6 \pm 0.2$	0.013	$4110 \pm 120$	$9.52 \pm 0.40$	$0.51 \pm 0.01$	$3.6 \pm 2.0$
QSO 0056-36	00:58:37.0	-36:06:06	0.165	1.94	$1.62 \pm 0.51$	0.014	$4550 \pm 250$	$27.3 \pm 0.7$	$19.8 \pm 0.3$	$5.44 \pm 2.47$
RX J0100-51	01:00:27.0	-51:13:55	0.062	2.42	$1.75 \pm 0.52$	0.015	$3190 \pm 630$	$27.2 \pm 0.8$	$19.7 \pm 0.3$	$10.2 \pm 4.8$
MS 0117-28	01:19:36.0	-28:21:31	0.349	1.65	$2.51 \pm 0.66$	0.017	$1681 \pm 260$	$15.4 \pm 0.5$	$12.5 \pm 0.2$	$1.51 \pm 1.45$
RX J0134-42	01:34:17.0	-42:58:27	0.237	1.59	$6.7 \pm 2.6$	0.017	$1160 \pm 80$	$17.0 \pm 0.6$	$16.7 \pm 0.3$	$(3 \times 10^{-5}) \pm 10^{-2}$
RX J0136-35	01:36:54.0	-35:09:53	0.289	5.60	$4.9 \pm 0.5$	0.016	$1320 \pm 120$	$7.15 \pm 0.34$	$5.02 \pm 0.13$	$(2.04 \pm 4.38) \times 10^{-2}$
RX J0148-27	01:48:22.0	-27:58:26	0.121	1.50	$2.62 \pm 0.30$	0.017	$1030 \pm 100$	$20.4 \pm 0.5$	$17.2 \pm 0.2$	$7.25 \pm 1.89$
RX J0152-23	01:52:27.0	-23:19:54	0.113	1.10	$1.75 \pm 0.39$	0.012	$2890 \pm 250$	$18.2 \pm 0.6$	$13.9 \pm 0.2$	$6.20 \pm 1.68$
Mrk 1048	02:34:37.8	-08:47:16	0.042	2.90	$1.67 \pm 0.43$	0.033	$5670 \pm 160$	$44.1 \pm 0.1$	$35.08 \pm 0.06$	$18.9 \pm 7.5$
RX J0323-49	03:23:15.0	-49:31:51	0.071	1.72	$2.35 \pm 0.29$	0.017	$1680 \pm 250$	$51.0 \pm 0.2$	$40.16 \pm 0.09$	$6.04 \pm 1.54$
Fairall 1116	03:51:42.0	-40:28:00	0.059	3.84	$1.87 \pm 0.53$	0.013	$4310 \pm 630$	$1.24 \pm 0.15$	$2.62 \pm 0.09$	$8.78 \pm 4.32$
RX J0435-46	04:35:14.0	-46:15:33	0.070	1.80	$2.2 \pm 0.3$	0.014	$3820 \pm 240$	$28.9 \pm 0.7$	$22.0 \pm 0.3$	$1.17 \pm 1.15$
RX J0435-36	04:35:54.0	-36:36:41	0.141	1.49	$1.6 \pm 0.2$	0.013	$6750 \pm 620$	$4.68 \pm 0.27$	$4.57 \pm 0.13$	$3.63 \pm 1.27$
H0439-27	04:41:22.5	-27:08:20	0.084	2.50	$1.30 \pm 1.57$	0.036	$2550 \pm 150$	$7.44 \pm 0.27$	$6.90 \pm 0.16$	$8.65 \pm 4.72$
RX J0454-48	04:54:43.0	-48:13:20	0.363	1.91	$2.4 \pm 0.7$	0.011	$1970 \pm 200$	$3.66 \pm 0.23$	$5.40 \pm 0.13$	$2.50 \pm 1.07$
RX J0902-07	09:02:33.6	-07:00:04	0.089	3.31	$2.12 \pm 0.62$	0.037	$1860 \pm 150$	$2.43 \pm 0.21$	$2.40 \pm 0.09$	$4.05 \pm 2.06$
RX J1005+43	10:05:42.0	+43:32:41	0.178	1.08	$2.15 \pm 0.46$	0.011	$2990 \pm 120$	$3.33 \pm 0.25$	$2.90 \pm 0.11$	$3.16 \pm 1.78$
RX J1007+22	10:07:10.2	+22:03:02	0.083	2.76	$2.91 \pm 0.54$	0.031	$2740 \pm 250$	$14.5 \pm 0.5$	$12.3 \pm 0.2$	$7.28 \pm 3.42$
CBS 126	10:13:03.0	+35:51:24	0.079	1.41	$1.62 \pm 0.33$	0.011	$2980 \pm 200$	$2.84 \pm 0.21$	$2.97 \pm 0.10$	$10.1 \pm 2.7$
Mrk 141	10:19:13.0	+63:58:03	0.042	1.07	$1.84 \pm 0.58$	0.010	$3600 \pm 110$	$17.7 \pm 0.5$	$14.8 \pm 0.2$	$3.32 \pm 1.63$
Mrk 142	10:25:31.0	+51:40:35	0.045	1.18	$2.10 \pm 0.27$	0.016	$1620 \pm 120$	$9.46 \pm 0.40$	$10.2 \pm 0.2$	$4.61 \pm 1.13$
RX J1117+65	11:17:10.0	+65:22:07	0.147	0.91	$2.50 \pm 0.49$	0.012	$1650 \pm 170$	$22.3 \pm 0.6$	$16.7 \pm 0.2$	$1.91 \pm 1.17$
PG 1115+407	11:18:30.4	+40:25:55	0.154	1.91	$1.81 \pm 0.66$	0.016	$1740 \pm 180$	$5.71 \pm 0.25$	$6.77 \pm 0.13$	$2.48 \pm 1.46$
Mrk 734	11:21:47.0	+11:44:19	0.033	2.64	$2.0 \pm 0.2$	0.032	$2230 \pm 140$	$24.7 \pm 0.7$	$20.1 \pm 0.3$	$2.49 \pm 1.16$
MCG+08-23-067	12:36:51.2	+45:39:05	0.030	1.37	$1.36 \pm 0.53$	0.017	$730 \pm 140$	$47.1 \pm 0.7$	$38.9 \pm 0.3$	$6.45 \pm 3.21$
IC 3599	12:37:41.0	+26:42:28	0.021	3.77	$3.37 \pm 0.21$	0.019	$635 \pm 110$	$3.91 \pm 0.27$	$3.98 \pm 0.13$	$6.45 \pm 3.21$
NGC 4593	12:39:39.4	-05:20:39	0.009	2.33	$1.19 \pm 0.42$	0.025	$4910 \pm 300$	$(4.85 \pm 2.11) \times 10^{-2}$	$0.41 \pm 0.04$	$5.88 \pm 1.39$
IRASF 1239+33	12:42:11.0	+33:17:03	0.044	1.35	$2.02 \pm 0.42$	0.019	$1640 \pm 250$	$50.5 \pm 0.9$	$55.8 \pm 0.4$	$46.5 \pm 18.9$
PG 1244+026	12:46:35.2	+02:22:09	0.049	1.75	$1.44 \pm 0.53$	0.026	$830 \pm 50$	$1.14 \pm 0.13$	$1.79 \pm 0.08$	$2.87 \pm 0.86$
RX J1304+05	13:04:17.0	+02:05:37	0.229	1.77	$2.26 \pm 0.59$	0.024	$1300 \pm 800$	$12.9 \pm 0.1$	$11.84 \pm 0.04$	$8.39 \pm 4.41$
RX J1312+26	13:12:59.0	+26:28:27	0.061	1.10	$1.5 \pm 0.2$	0.012	$2905 \pm 220$	$5.12 \pm 0.27$	$3.44 \pm 0.11$	$1.72 \pm 1.05$
RX J1319+52	13:19:57.1	+52:35:33	0.092	1.19	$2.06 \pm 0.44$	0.016	$950 \pm 100$	$5.57 \pm 0.34$	$4.47 \pm 0.14$	$4.48 \pm 2.45$
								$1.15 \pm 0.15$	$1.27 \pm 0.07$	$4.68 \pm 2.50$

Table 1—Continued

Name	$\alpha_{2000}$	$\delta_{2000}$	z	$N_{\text{H}}$ [ $10^{20} \text{cm}^{-2}$ ]	$\alpha_{\text{x}}$	E(B - V)	FWHM(H $\beta$ ) [ $\text{km s}^{-1}$ ]	$\nu F_{\nu}(1582 \text{ \AA})$ [ $10^{-12} \text{erg s}^{-1} \text{cm}^{-2}$ ]	$\nu F_{\nu}(2271 \text{ \AA})$ [ $10^{-12} \text{erg s}^{-1} \text{cm}^{-2}$ ]	$F_{\nu}(2 \text{ keV})$ [ $10^{-13} \text{erg s}^{-1} \text{cm}^{-2} \text{keV}^{-1}$ ]
RX J1355+56	13:55:17.0	+56:12:45	0.122	1.15	$2.31 \pm 0.42$	0.008	$1110 \pm 100$	$6.62 \pm 0.38$	$7.20 \pm 0.17$	$2.55 \pm 1.52$
RX J1413+70	14:13:37.0	+70:29:51	0.107	1.93	$1.07 \pm 0.47$	0.016	$4400 \pm 1000$	$0.21 \pm 0.06$	$0.18 \pm 0.03$	$10.3 \pm 2.8$
Mrk 478	14:42:08.0	+35:26:23	0.077	1.04	$2.22 \pm 0.16$	0.014	$1630 \pm 150$	$45.3 \pm 1.0$	$39.0 \pm 0.4$	$7.04 \pm 1.76$
SBS 1527+56	15:29:07.5	+56:16:07	0.100	1.29	1.46 <sup>a</sup>	0.011	$2760 \pm 420$	$23.7 \pm 0.8$	$14.1 \pm 0.3$	$7.37 \pm 3.61$
KUG 1618+40	16:19:51.3	+40:58:48	0.038	0.93	$1.87 \pm 0.45$	0.007	$1820 \pm 100$	$4.86 \pm 0.34$	$3.28 \pm 0.13$	$3.90 \pm 2.30$
EXO 1627+40	16:29:01.3	+40:08:00	0.272	0.85	$2.15 \pm 0.37$	0.009	$1450 \pm 200$	$4.33 \pm 0.32$	$3.80 \pm 0.12$	$1.25 \pm 0.77$
RX J2144-39	21:44:49.2	-39:49:01	0.140	4.89	$3.4 \pm 0.3$	0.023	$1445 \pm 120$	$1.30 \pm 0.17$	$1.45 \pm 0.08$	$2.58 \pm 1.99$
NGC 7214	22:09:07.6	-27:48:36	0.023	1.64	$1.02 \pm 0.63$	0.019	$4700 \pm 250$	$20.7 \pm 0.5$	$17.8 \pm 0.2$	$10.4 \pm 5.2$
RX J2213-17	22:13:00.0	-17:10:18	0.146	2.48	$2.4 \pm 0.4$	0.026	$1625 \pm 200$	$5.29 \pm 0.27$	$4.44 \pm 0.12$	$1.51 \pm 1.90$
RX J2216-44	22:16:53.0	-44:51:57	0.136	2.17	$1.98 \pm 0.38$	0.018	$1630 \pm 130$	$19.1 \pm 0.5$	$14.0 \pm 0.2$	$3.13 \pm 1.72$
PKS 2227-399	22:30:40.3	-39:42:52	0.318	1.25	$0.72 \pm 0.55$	0.018	$3710 \pm 1500$	$7.66 \pm 0.38$	$5.82 \pm 0.16$	$10.6 \pm 5.1$
RX J2232-41	22:32:43.0	-41:34:37	0.075	1.60	$1.8 \pm 0.5$	0.013	$4490 \pm 350$	$3.50 \pm 0.23$	$2.74 \pm 0.10$	$1.31 \pm 2.46$
RX J2241-44	22:41:56.0	-44:04:55	0.545	1.76	$2.5 \pm 0.4$	0.011	$1890 \pm 200$	$11.7 \pm 0.4$	$12.5 \pm 0.2$	$0.68 \pm 1.00$
RX J2242-38	22:42:38.0	-38:45:17	0.221	1.18	$2.92 \pm 0.70$	0.014	$1900 \pm 200$	$8.35 \pm 0.40$	$5.46 \pm 0.15$	$1.22 \pm 1.24$
MS 2254-37	22:57:39.0	-36:06:07	0.039	1.15	$1.84 \pm 0.43$	0.016	$1530 \pm 120$	$(9.49 \pm 4.22) \times 10^{-2}$	$0.143 \pm 0.022$	$5.50 \pm 1.49$
RX J2304-51	23:04:39.0	-51:27:59	0.106	1.33	$3.2 \pm 0.2$	0.008	$1775 \pm 130$	$2.10 \pm 0.19$	$1.36 \pm 0.07$	$1.96 \pm 1.95$
RX J2312-34	23:12:34.8	-34:04:20	0.202	1.74	$0.78 \pm 1.13$	0.017	$4200 \pm 950$	$9.85 \pm 0.40$	$6.62 \pm 0.15$	$6.65 \pm 3.84$
RX J2317-44	23:17:50.0	-44:22:27	0.132	1.89	$2.50 \pm 0.80$	0.010	$1010 \pm 150$	$6.24 \pm 0.34$	$5.43 \pm 0.15$	$0.69 \pm 1.03$
RX J2340-53	23:40:23.0	-53:28:57	0.321	1.18	$2.1 \pm 0.6$	0.012	$1565 \pm 80$	$5.12 \pm 0.30$	$3.32 \pm 0.01$	$0.76 \pm 2.12$
RX J2349-31	23:49:24.0	-31:26:03	0.135	1.23	$1.55 \pm 0.57$	0.010	$4200 \pm 2000$	$2.31 \pm 0.21$	$2.07 \pm 0.09$	$3.97 \pm 2.26$

<sup>a</sup>Taken from Grupe et al. (2004), who do not list uncertainties.

Note. — Blank lines indicate an additional GALEX observation of the object on the preceding line. UV fluxes were extracted from GALEX plates using the IRAF *phot* package. Equatorial coordinates and FWHM come from Grupe et al. (2004) where possible and from Grupe et al. (1999) otherwise. Color excesses come from Simbad, and  $N_{\text{H}}$  values were extracted from Dickey & Lockman (1990). X-ray indices and count rates were taken from Grupe et al. (2001) wherever possible and from Grupe et al. (1998) otherwise. All other parameters come from Grupe et al. (1998). The names used here, following the naming convention of Grupe et al. (1998), differ from the object names included in the ROSAT All-Sky Catalog for the same objects.

Table 2. Re-classified Broad-Line Seyfert Galaxies

Object	FWHM(H $\beta$ )[km s $^{-1}$ ]		$\alpha_x$
	Grupe et al. (1999)	Grupe et al. (2004)	
MS0117-28	2925 $\pm$ 100	1681 $\pm$ 260	2.51 $\pm$ 0.66
RXJ0323-49	2075 $\pm$ 250	1680 $\pm$ 250	2.03 $\pm$ 0.10
RXJ1117+65	2160 $\pm$ 110	1650 $\pm$ 170	2.50 $\pm$ 0.49
RXJ2216-44	2200 $\pm$ 130	1630 $\pm$ 130	1.98 $\pm$ 0.38
Mrk734	2230 $\pm$ 140	—	2.0 $\pm$ 0.2

Table 3. Physical Correlations (Bentz Masses)

Parameters		NLS1		BLS1		Merged	
		$r_S$	Prob.	$r_S$	Prob.	$r_S$	Prob.
$\nu F_\nu(1528\text{\AA})/\nu F_\nu(2\text{keV})$	$M_{BH}$	0.47	0.10	0.20	0.54	0.10	0.64
$\nu F_\nu(1528\text{\AA})/\nu F_\nu(2\text{keV})$	$L/L_{\text{edd}}$	0.61	0.027	0.36	0.55	0.36	0.054
$\nu F_\nu(1528\text{\AA})/\nu F_\nu(2\text{keV})$	$\nu L_\nu(1528\text{\AA})$	0.92	$2.2 \times 10^{-12}$	0.39	0.052	0.74	$2.3 \times 10^{-10}$
$\nu F_\nu(1528\text{\AA})/\nu F_\nu(2\text{keV})$	$\nu L_\nu(5100\text{\AA})$	0.82	$7.2 \times 10^{-8}$	0.13	0.59	0.60	$1.9 \times 10^{-6}$
$\nu F_\nu(1528\text{\AA})/\nu F_\nu(2271\text{\AA})$	$M_{BH}$	0.44	0.14	0.48	0.052	0.59	$6.6 \times 10^{-4}$
$\nu F_\nu(1528\text{\AA})/\nu F_\nu(2271\text{\AA})$	$L/L_{\text{edd}}$	0.53	0.065	0.34	0.54	-0.13	0.56
$\nu F_\nu(1528\text{\AA})/\nu F_\nu(2271\text{\AA})$	$\nu L_\nu(1528\text{\AA})$	0.52	$3.5 \times 10^{-3}$	0.61	$1.2 \times 10^{-3}$	0.48	$2.4 \times 10^{-4}$
$\nu F_\nu(1528\text{\AA})/\nu F_\nu(2271\text{\AA})$	$\nu L_\nu(5100\text{\AA})$	0.39	0.037	0.37	0.067	0.35	$9.7 \times 10^{-3}$
$\alpha_x$	$M_{BH}$	0.48	0.10	0.05	0.84	-0.43	0.019
$\alpha_x$	$L/L_{\text{edd}}$	0.27	0.50	0.14	0.63	0.53	$2.7 \times 10^{-3}$
$\alpha_x$	$\nu L_\nu(1528\text{\AA})$	0.55	$1.9 \times 10^{-3}$	0.12	0.62	0.31	0.022
$\alpha_x$	$\nu L_\nu(5100\text{\AA})$	0.49	$7.0 \times 10^{-3}$	0.12	0.61	0.28	0.038
FWHM(H $\beta$ )	$M_{BH}$	0.83	$4.7 \times 10^{-4}$	0.64	$5.4 \times 10^{-3}$	0.90	$1.0 \times 10^{-11}$
FWHM(H $\beta$ )	$L/L_{\text{edd}}$	-0.54	0.027	-0.20	0.57	-0.80	$8.8 \times 10^{-8}$
FWHM(H $\beta$ )	$\nu L_\nu(1528\text{\AA})$	0.32	0.094	0.03	0.88	0.045	0.75
FWHM(H $\beta$ )	$\nu L_\nu(5100\text{\AA})$	0.36	0.055	-0.03	0.88	0.08	0.59
FWHM(H $\beta$ )	$M_{BH}/\dot{m}$	0.62	0.023	0.84	$2.2 \times 10^{-5}$	0.94	$1.0 \times 10^{-14}$
$M_{BH}$	$L/L_{\text{edd}}$	-0.04	0.89	0.14	0.63	-0.59	$5.8 \times 10^{-4}$
$M_{BH}$	$\nu L_\nu(5100\text{\AA})$	0.90	$2.8 \times 10^{-5}$	0.54	0.025	0.53	$2.6 \times 10^{-3}$
$L/L_{\text{edd}}$	$\nu L_\nu(5100\text{\AA})$	0.044	0.89	0.14	0.63	-0.59	$5.8 \times 10^{-4}$

Table 4. Physical Correlation Results

Parameters		NLS1		BLS1		Merged	
		$r_s$	Prob.	$r_s$	Prob.	$r_s$	Prob.
$\nu F_\nu(1528\text{\AA})/\nu F_\nu(2\text{keV})$	$M_{BH}$	0.53	0.065	0.52	0.03	0.28	0.60
$\nu F_\nu(1528\text{\AA})/\nu F_\nu(2\text{keV})$	$L/L_{\text{edd}}$	0.55	0.050	0.16	0.59	0.29	0.62
$\nu F_\nu(1528\text{\AA})/\nu F_\nu(2\text{keV})$	$\nu L_\nu(1528\text{\AA})$	0.92	$2.2 \times 10^{-12}$	0.39	0.052	0.74	$2.3 \times 10^{-10}$
$\nu F_\nu(1528\text{\AA})/\nu F_\nu(2\text{keV})$	$\nu L_\nu(5100\text{\AA})$	0.82	$7.2 \times 10^{-8}$	0.13	0.59	0.60	$1.9 \times 10^{-6}$
$\nu F_\nu(1528\text{\AA})/\nu F_\nu(2271\text{\AA})$	$M_{BH}$	0.47	0.10	0.26	0.50	0.44	0.016
$\nu F_\nu(1528\text{\AA})/\nu F_\nu(2271\text{\AA})$	$L/L_{\text{edd}}$	0.44	0.13	0.57	0.017	-0.06	0.74
$\nu F_\nu(1528\text{\AA})/\nu F_\nu(2271\text{\AA})$	$\nu L_\nu(1528\text{\AA})$	0.52	$3.5 \times 10^{-3}$	0.61	$1.2 \times 10^{-3}$	0.48	$2.4 \times 10^{-4}$
$\nu F_\nu(1528\text{\AA})/\nu F_\nu(2271\text{\AA})$	$\nu L_\nu(5100\text{\AA})$	0.39	0.037	0.37	0.067	0.35	$9.7 \times 10^{-3}$
$\alpha_x$	$M_{BH}$	0.51	0.079	0.28	0.50	-0.28	0.60
$\alpha_x$	$L/L_{\text{edd}}$	0.21	0.55	0.14	0.62	0.49	$5.8 \times 10^{-3}$
$\alpha_x$	$\nu L_\nu(1528\text{\AA})$	0.55	$1.9 \times 10^{-3}$	0.12	0.62	0.31	0.022
$\alpha_x$	$\nu L_\nu(5100\text{\AA})$	0.49	$7.0 \times 10^{-3}$	0.12	0.61	0.28	0.038
FWHM(H $\beta$ )	$M_{BH}$	0.82	$6.5 \times 10^{-4}$	0.42	0.097	0.77	$7.7 \times 10^{-7}$
FWHM(H $\beta$ )	$L/L_{\text{edd}}$	-0.39	0.53	-0.47	0.060	-0.79	$2.7 \times 10^{-7}$
FWHM(H $\beta$ )	$\nu L_\nu(1528\text{\AA})$	0.32	0.094	0.03	0.88	0.045	0.75
FWHM(H $\beta$ )	$\nu L_\nu(5100\text{\AA})$	0.36	0.055	-0.03	0.88	0.08	0.59
FWHM(H $\beta$ )	$M_{BH}/\dot{m}_{\text{edd}}$	0.87	$1.1 \times 10^{-4}$	0.76	$3.6 \times 10^{-4}$	0.89	$6.7 \times 10^{-11}$
$M_{BH}$	$L/L_{\text{edd}}$	-0.14	0.66	0.08	0.77	-0.53	$2.8 \times 10^{-3}$
$M_{BH}$	$\nu L_\nu(5100\text{\AA})$	0.92	$7.6 \times 10^{-6}$	0.63	$7.1 \times 10^{-3}$	0.63	$2.1 \times 10^{-4}$
$L/L_{\text{edd}}$	$\nu L_\nu(5100\text{\AA})$	0.05	0.87	0.63	$6.3 \times 10^{-3}$	0.14	0.55

Table 5. Observable Correlation Results

Parameters		NLS1		BLS1		Merged	
		$r_s$	Prob.	$r_s$	Prob.	$r_s$	Prob.
$\nu F_\nu(1528\text{\AA})/\nu F_\nu(2\text{keV})$	$\alpha_x$	0.90	$7.6 \times 10^{-11}$	0.56	$1.6 \times 10^{-3}$	0.53	$3.8 \times 10^{-5}$
$\nu F_\nu(1528\text{\AA})/\nu F_\nu(2\text{keV})$	$\nu F_\nu(1528\text{\AA})/\nu F_\nu(2271\text{\AA})$	0.52	$3.7 \times 10^{-3}$	0.23	0.51	0.37	$5.8 \times 10^{-3}$
$\nu F_\nu(1528\text{\AA})/\nu F_\nu(2\text{keV})$	FWHM(H $\beta$ )	0.34	0.076	-0.19	0.51	-0.05	0.71
$\nu F_\nu(1528\text{\AA})/\nu F_\nu(2271\text{\AA})$	$\alpha_x$	-0.26	0.55	0.06	0.78	-0.19	0.57
$\nu F_\nu(1528\text{\AA})/\nu F_\nu(2271\text{\AA})$	FWHM(H $\beta$ )	-0.41	0.029	-0.03	0.88	-0.03	0.81
$\alpha_x$	FWHM(H $\beta$ )	0.33	0.88	-0.14	0.61	-0.53	$4.1 \times 10^{-5}$

Note. — Here  $r_s$  is the Spearman rank order correlation coefficient, and Prob. is the probability for  $r_s$  to appear at random in two data sets drawn from two uncorrelated variables.

Table 6. Properties of Outliers

	$z$	$\alpha_x$	$\alpha_{\text{ox}}$	$N_H$ $\text{cm}^{-2}$	FWHM(H $\beta$ ) $\text{km s}^{-1}$	$\log(L_x)$ $\text{erg s}^{-1}$	$\log(\lambda L_\lambda(1528\text{\AA}))$ $\text{erg s}^{-1}$	$\log(\lambda L_\lambda(5100\text{\AA}))$ $\text{erg s}^{-1}$
RXJ0134-43	0.237	6.70	$3 \pm 82$	$1.6 \times 10^{20}$	$1160 \pm 80$	41.3	$45.44 \pm 0.02$	44.9
RXJ0136-35	0.289	4.90	$2.0 \pm 0.4$	$5.6 \times 10^{20}$	$1320 \pm 120$	43.9	$45.26 \pm 0.02$	44.4
RXJ0323-49	0.071	2.03	$1.17 \pm 0.06$	$1.72 \times 10^{20}$	$1680 \pm 250$	44.0	$43.16 \pm 0.05$	43.5
RXJ0902-07	0.089	2.17	$1.19 \pm 0.09$	$3.31 \times 10^{20}$	$1860 \pm 150$	44.1	$43.80 \pm 0.03$	43.3
IC3599	0.021	3.20	$0.9 \pm 0.1$	$3.77 \times 10^{20}$	$635 \pm 100$	42.7	$40.66 \pm 0.19$	42.6
IRASF1239+33	0.044	2.02	$1.21 \pm 0.06$	$1.35 \times 10^{20}$	$1640 \pm 250$	43.4	$42.69 \pm 0.50$	43.3
RXJ1413+70	0.107	1.40	$0.6 \pm 0.1$	$1.93 \times 10^{20}$	$4400 \pm 1000$	44.2	$42.77 \pm 0.13$	43.8
RXJ2144-39	0.140	3.40	$1.1 \pm 0.1$	$4.89 \times 10^{20}$	$1445 \pm 120$	43.5	$43.81 \pm 0.06$	43.7
MS2254-37	0.039	1.80	$0.7 \pm 0.1$	$1.15 \times 10^{20}$	$1530 \pm 120$	43.5	$41.50 \pm 0.19$	43.3

Note. —  $L_x$  is measured in the ROSAT band, from 0.2-2.0 keV (Grupe et al. 2004).  $L_\lambda(5100 \text{ \AA})$ , FWHM(H $\beta$ ),  $\alpha_x$  and redshift all come from Grupe et al. (2004) where possible and from Grupe et al. (1998) otherwise.

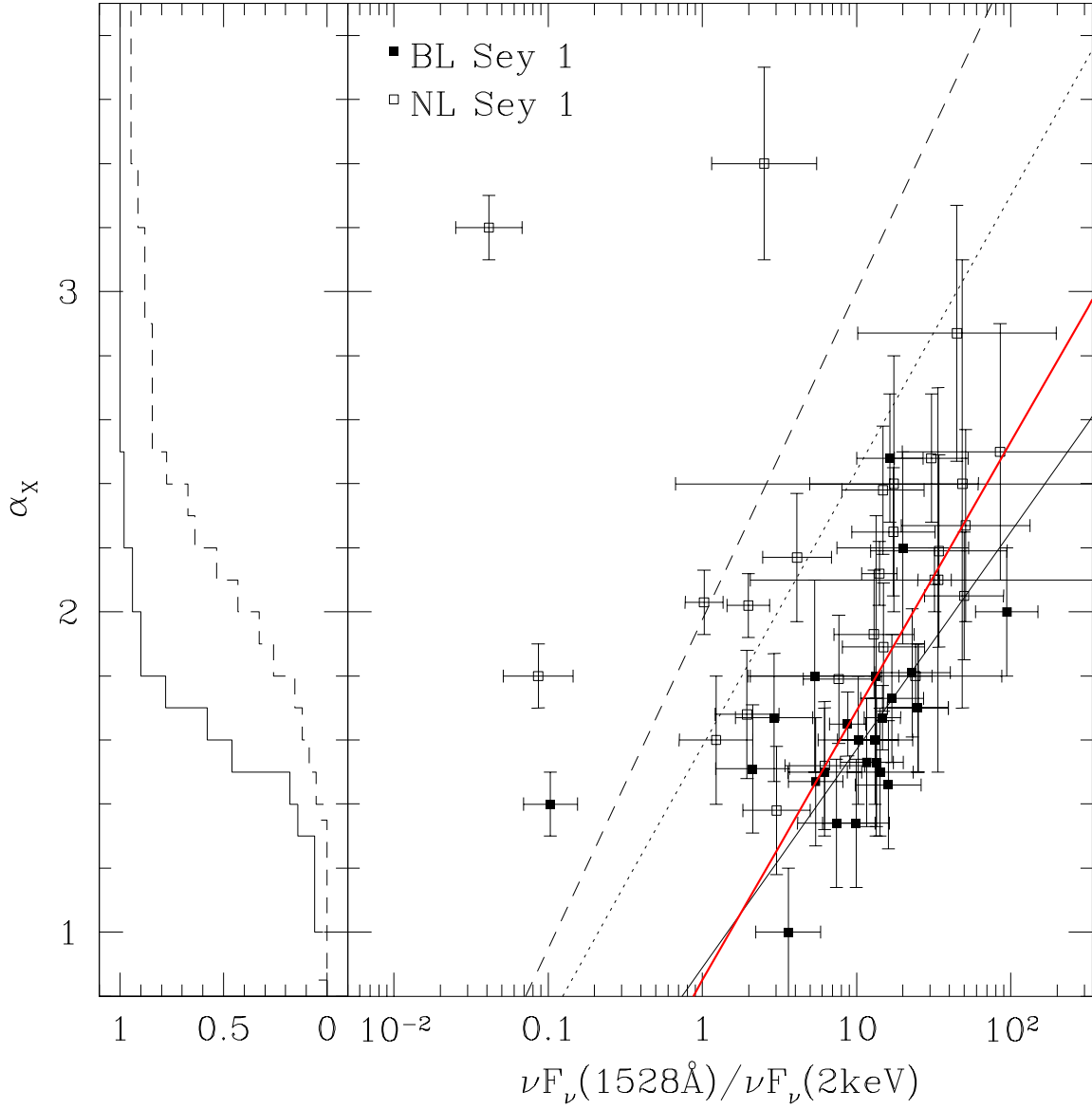


Fig. 1.— Comparison of two indicators for the strength of the soft X-ray excess. UV flux density is measured at the effective wavelength of the GALEX *FUV* band using the AB-magnitude relation. The *red* line is the best fit to our AGNs ( $\alpha_x = 0.84 \log[\nu F_\nu(1528 \text{ \AA})/\nu F_\nu(2 \text{ keV})] + 0.85$ ). The *solid* line is the best fit line to Figure 8 of Walter & Fink (1993), and the *dashed* line is a chi-by-eye fit to the outliers in the WF93 sample. The *dotted* line divides the “normal” sample of AGN from the outliers listed in Tab. 6. Our data indicate either weaker UV emission or steeper  $\alpha_x$  among our sample compared to WF93. The left panel compares the cumulative distributions of  $\alpha_x$  for the NLS1 (*dashed*) and BLS1 (*solid*) samples.

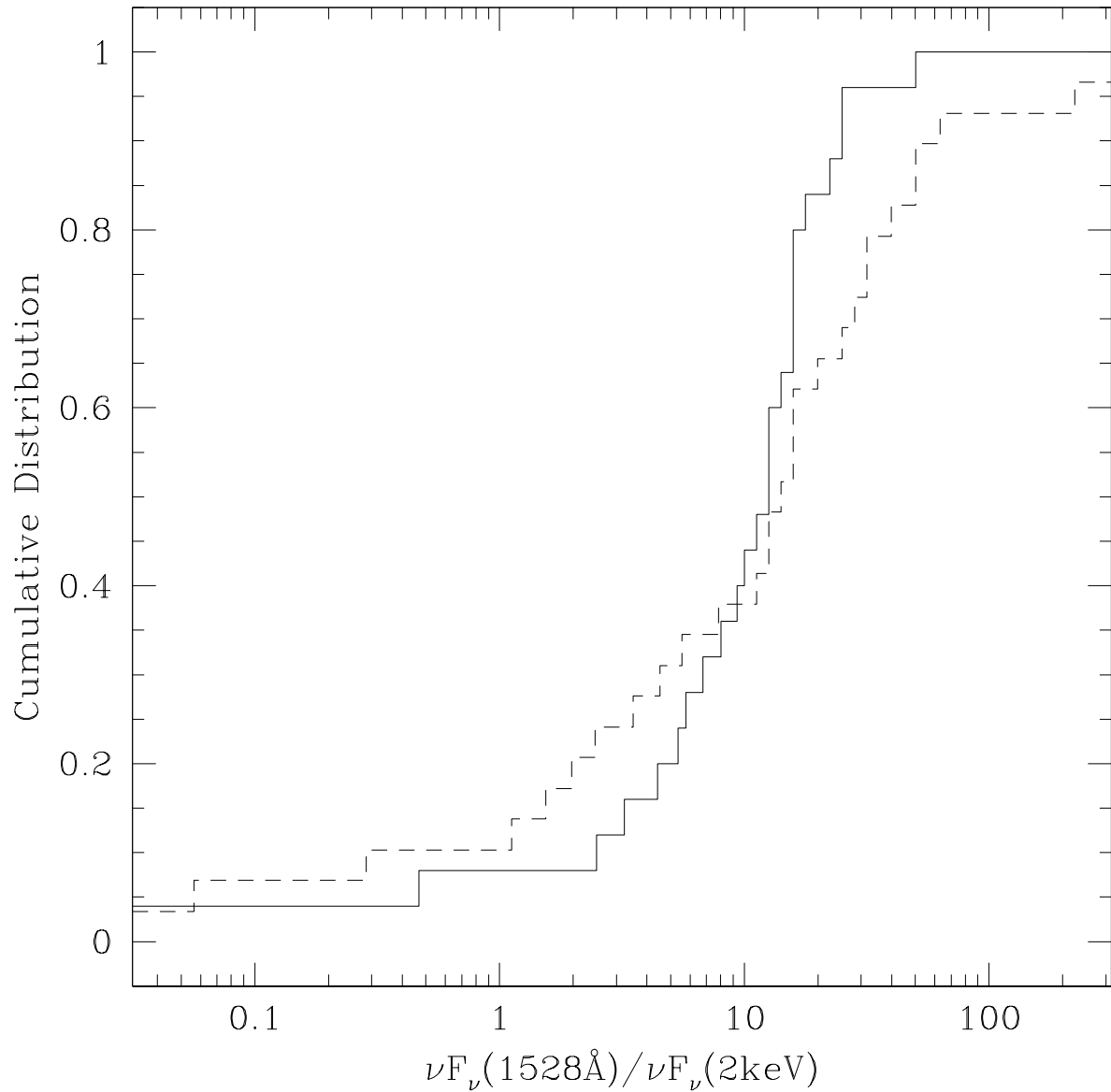


Fig. 2.— Comparison of the distributions of BBB strength for the BLS1 (*solid*) and NLS1 (*dashed*) samples. The two distributions are obviously similar near the median values (CDF=0.5), but differ significantly in the wings. The KS test using the Kuiper significance criterion yields a probability of 1.5% that the NLS1 and BLS1 samples are drawn from the same underlying population.

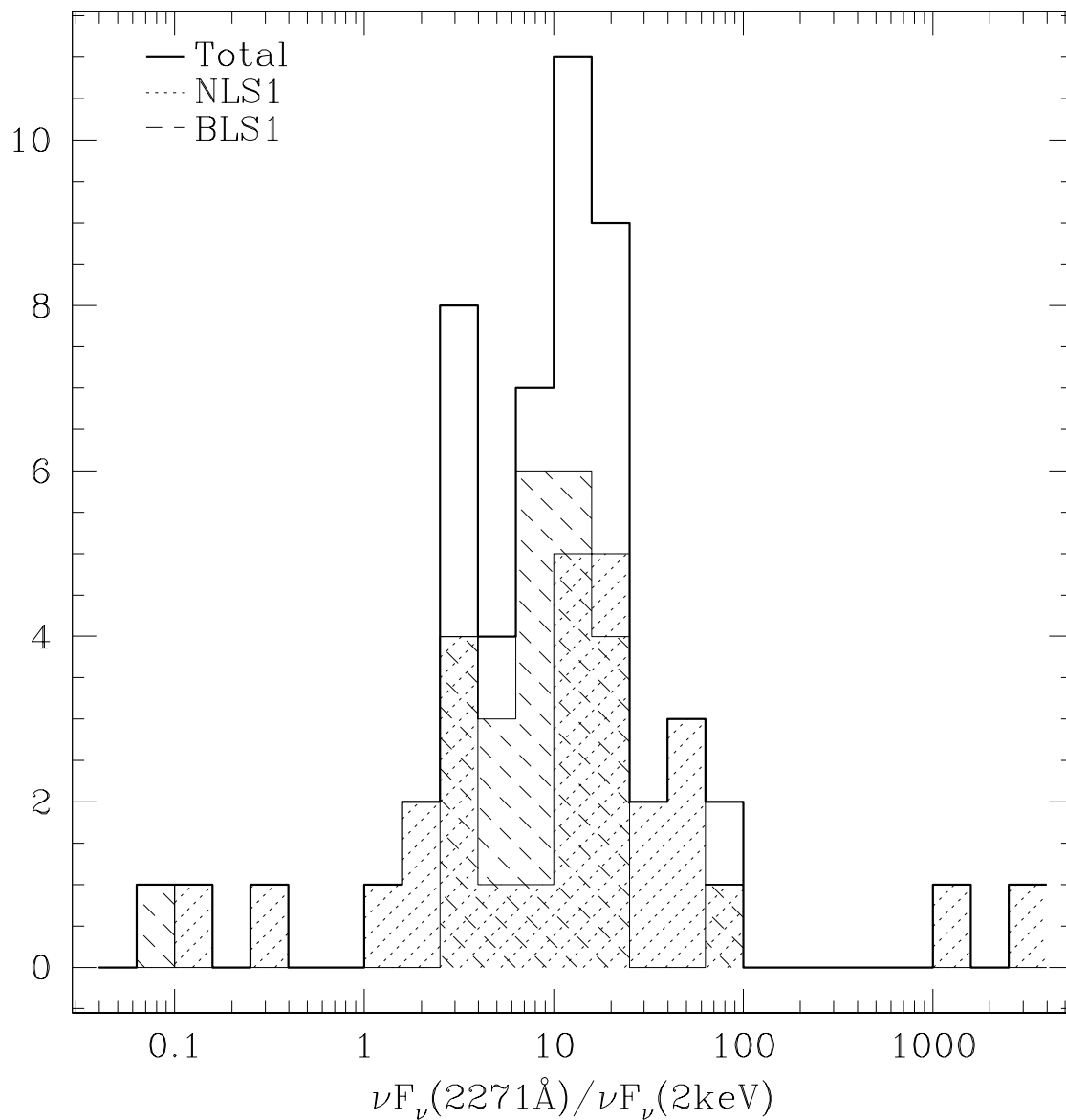


Fig. 3.— Distributions of *NUV* to X-ray flux ratios among the NLS1 (*dotted fill*) and BLS1 (*dashed fill*) samples. A flux ratio of 10 corresponds to  $\alpha_{\text{ox}} \approx 1.4$ . A KS-test yields a 5% probability that the two samples are drawn from the same parent population.

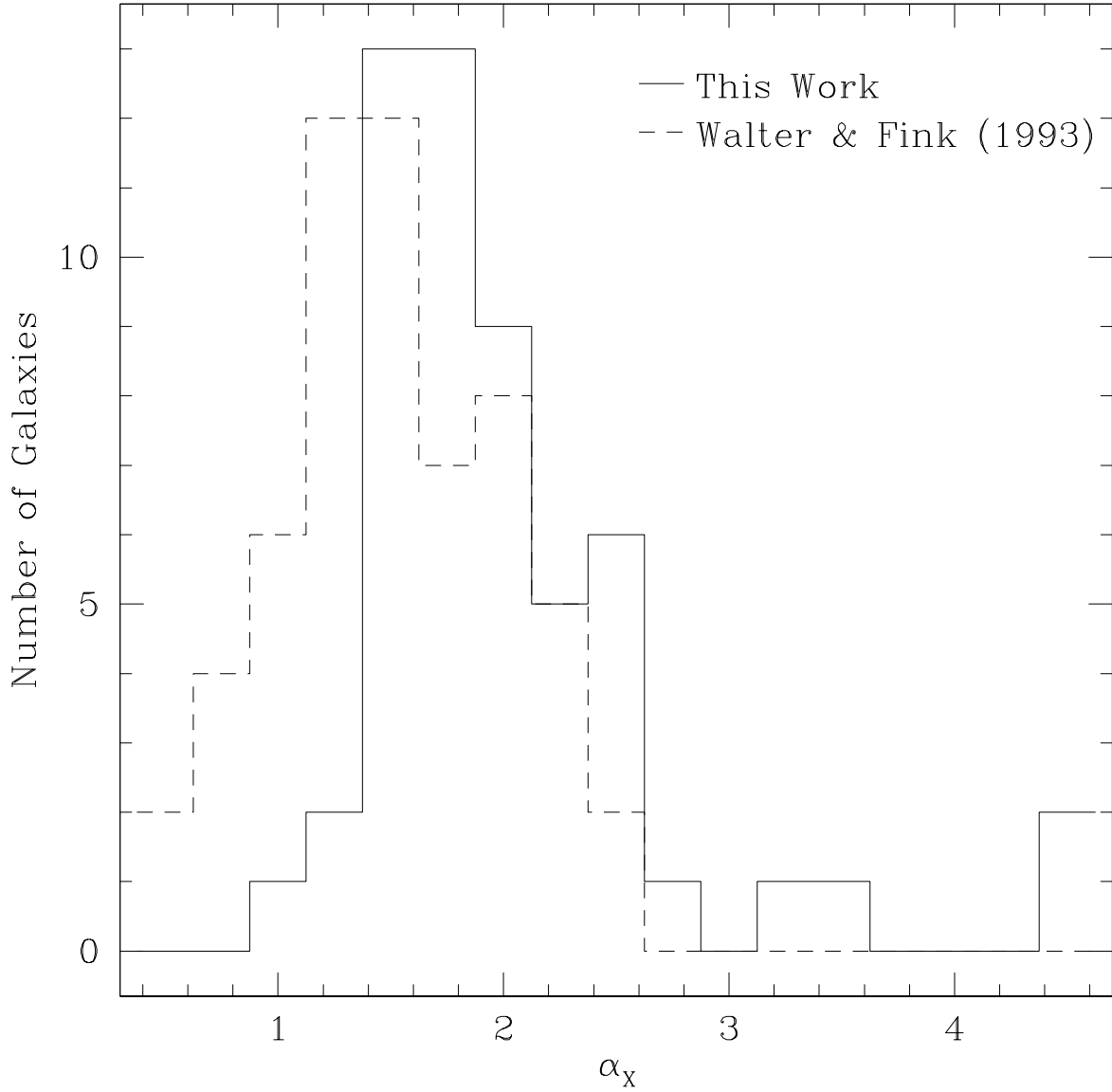


Fig. 4.— Comparison between X-ray spectral indices in Walter & Fink (1993) with the galaxies we examine. It is apparent that there is a significant preference for steeper soft X-ray spectra in our sample compared to that of WF93. Our sample also contains more objects with unusually soft X-ray spectra.

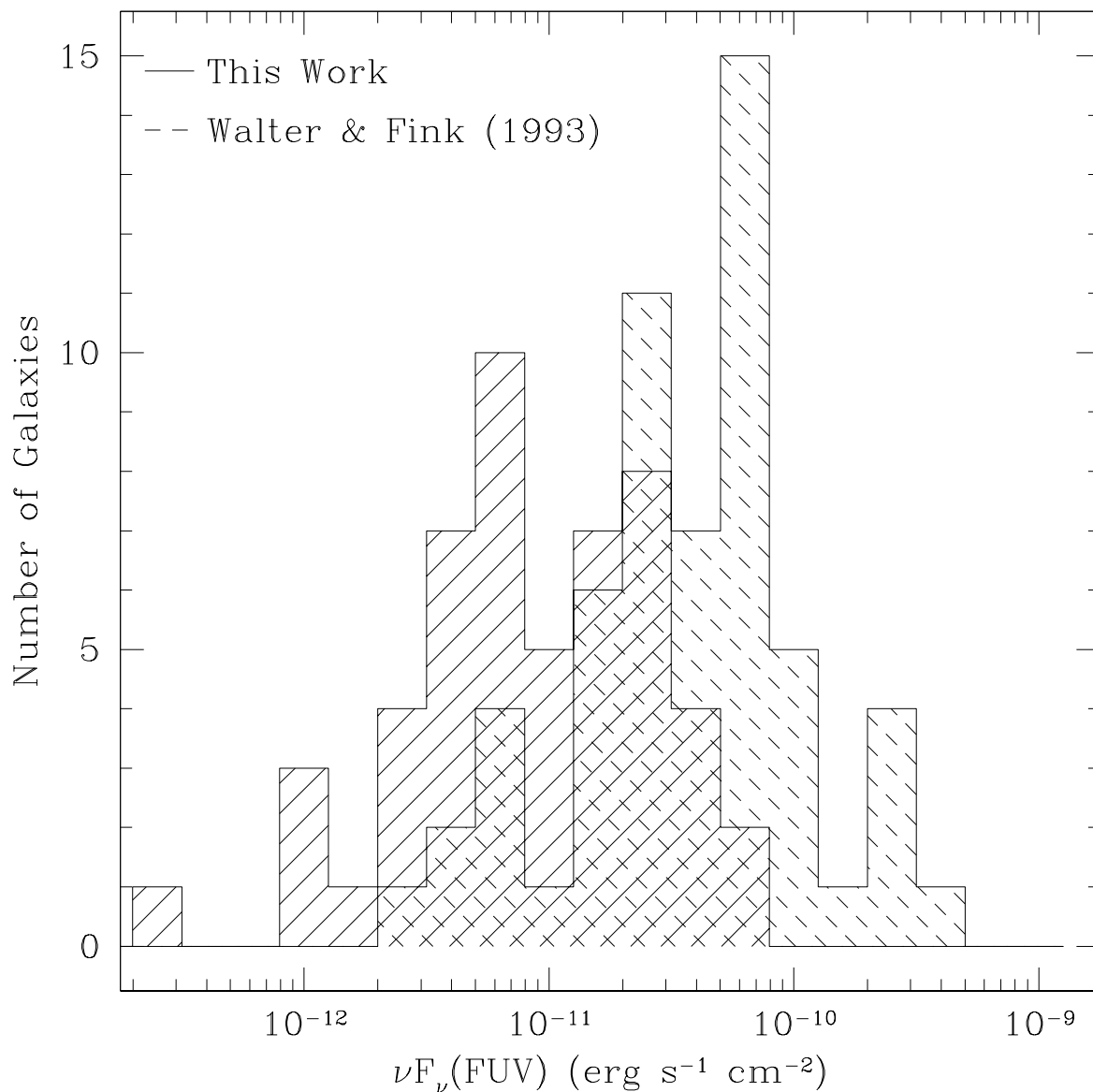


Fig. 5.— Comparison of the far-UV fluxes used in the Walter & Fink (1993; WF93) (*solid fill*) analysis and those used in our analysis (*dashed fill*). The two are not directly comparable, since WF93 measure far-UV fluxes at  $1375\text{\AA}$  while the center of the GALEX *FUV* band is at  $1528\text{\AA}$ , but the comparison is illuminating for to the analogy drawn in Fig. 1

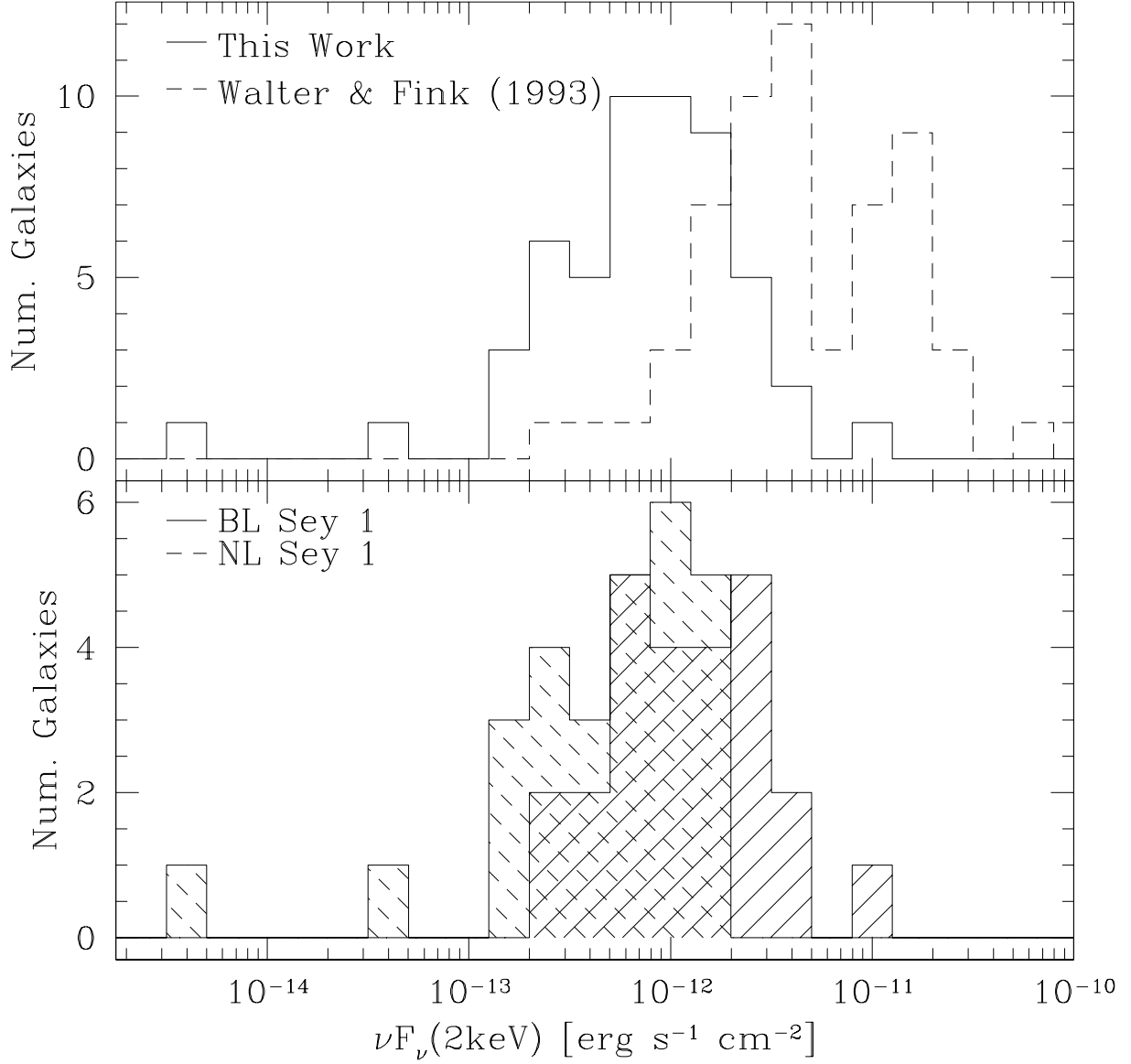


Fig. 6.— Distributions of 2keV fluxes in our BLS1 (*solid fill*) and NLS1 (*dashed fill*) samples (lower panel) and a comparison of our combined sample (*solid*) with that of Walter & Fink (1993; upper panel; *dashed*). Our sample extends to significantly lower  $\nu F_\nu(2\text{keV})$  than the Walter & Fink sample due to the steeper X-ray spectral indices in our objects.

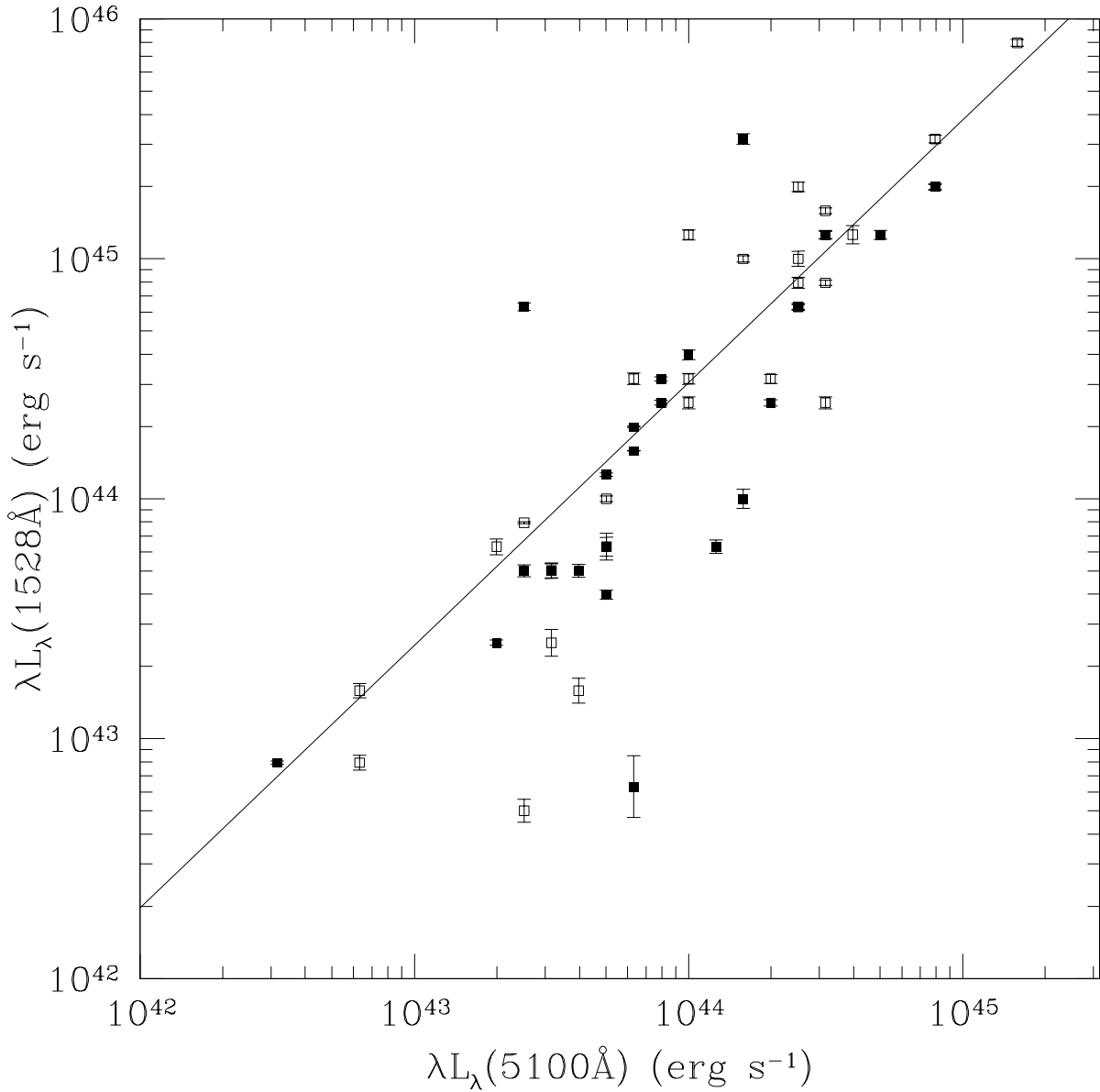


Fig. 7.— Correlation of *FUV* and *V*-band luminosities for both BLS1 (*filled*) and NLS1 (*open*) points. Objects with unusually low  $\lambda L_{\lambda}(1528 \text{ \AA})$  for their  $\lambda L_{\lambda}(5100 \text{ \AA})$  could result from obscuration, and abnormally large  $\lambda L_{\lambda}(1528 \text{ \AA})$  might indicate star formation.

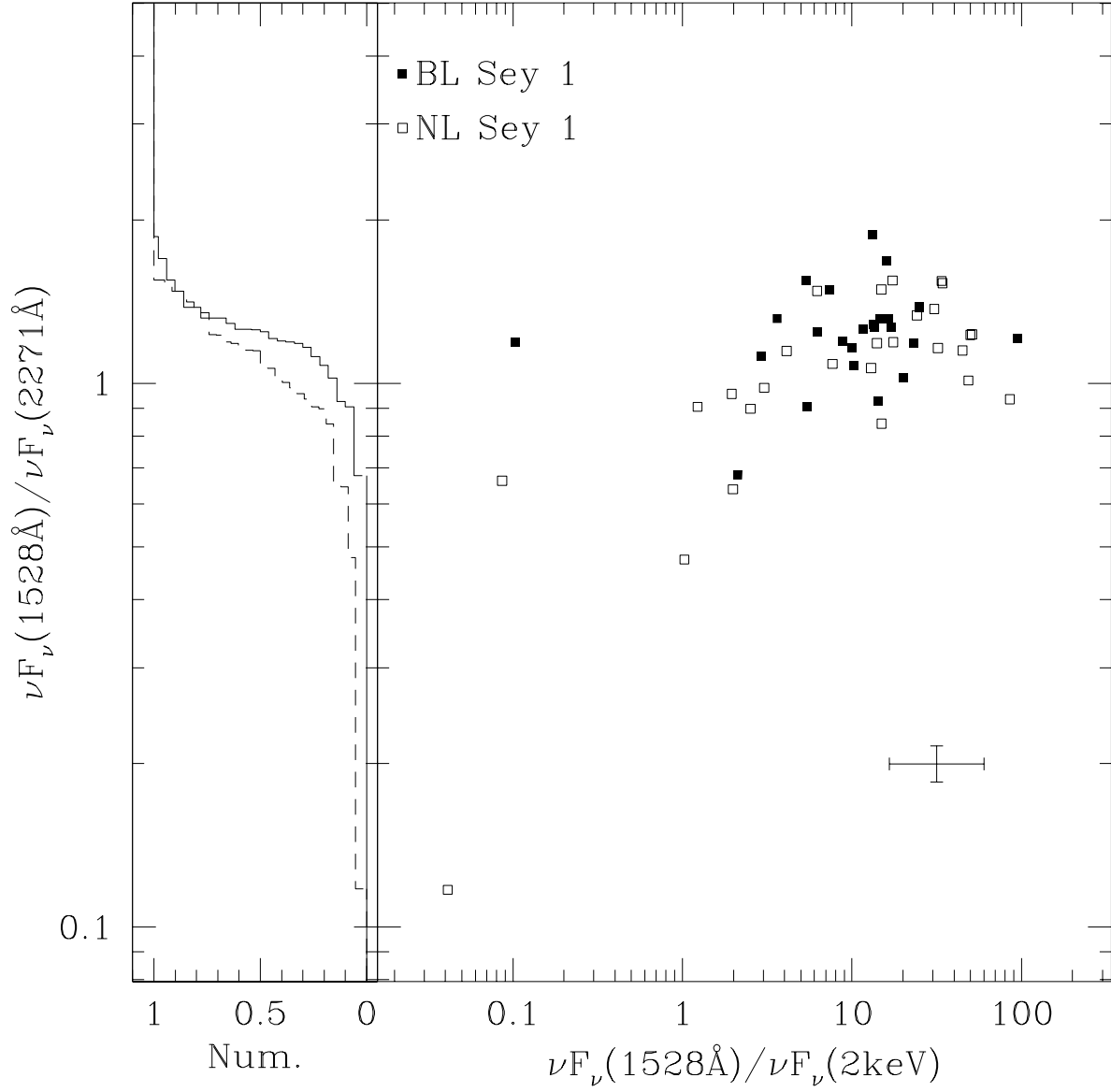


Fig. 8.— Relation between the shape  $\left(\nu F_\nu(1528 \text{ \AA})/\nu F_\nu(2271 \text{ \AA})\right)$  and strength  $\left(\nu F_\nu(1528 \text{ \AA})/\nu F_\nu(2 \text{ keV})\right)$  of the Big Blue Bump. The left panel shows the cumulative distributions of  $\nu F_\nu(1528 \text{ \AA})/\nu F_\nu(2271 \text{ \AA})$  in the BLS1 (*solid*) and NLS1 (*dashed*) samples. The cross in the lower right corner indicates typical error bars.

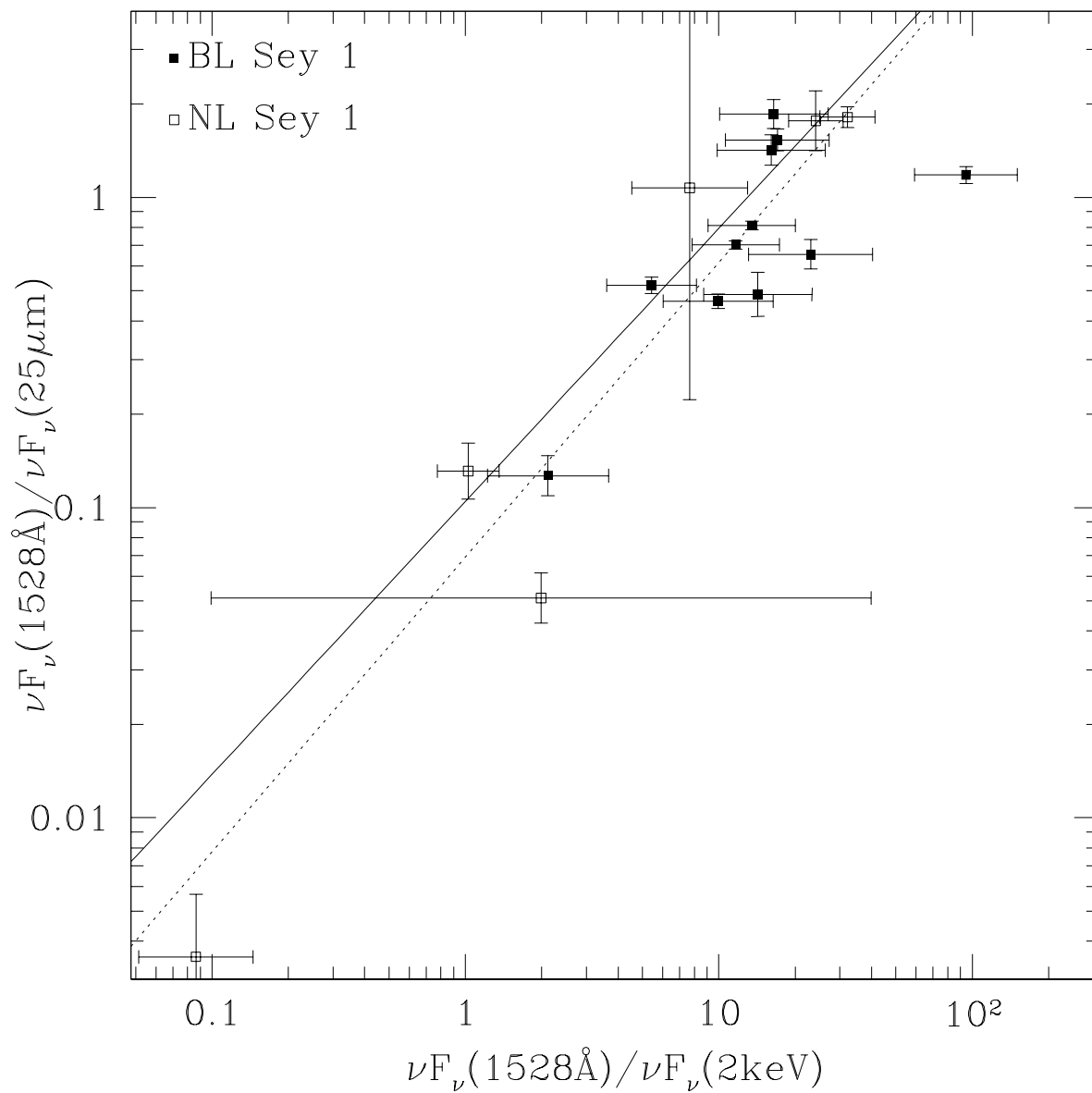


Fig. 9.— Relation between two indicators for the strength of Big Blue Bump with respect to the underlying, power-law continuum. The *solid* line marks the average relation between the two ratios reported by Walter & Fink (1993), and the *dotted* line indicates the best fit to our sample.

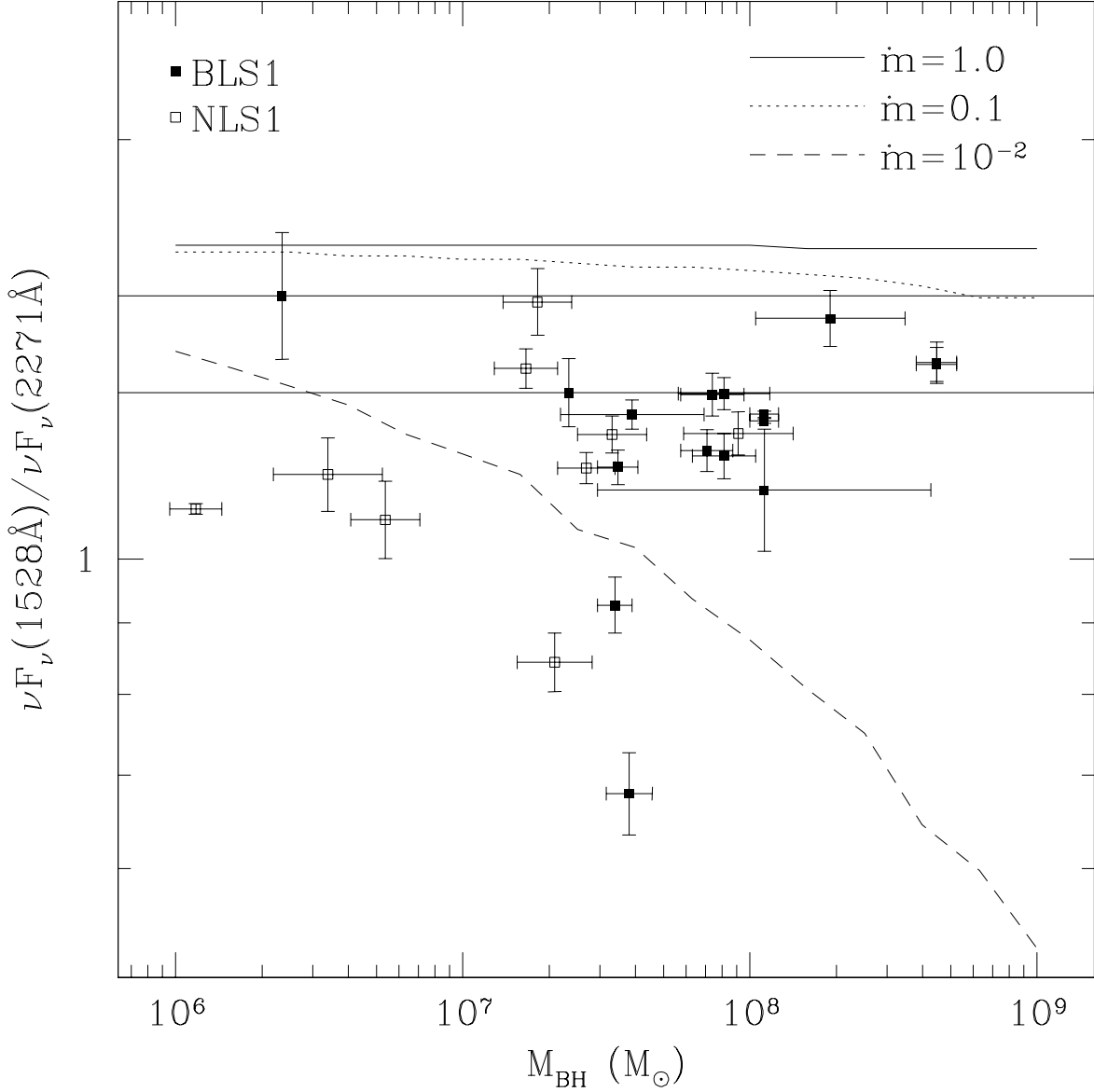


Fig. 10.— Rest-frame GALEX flux ratios for a standard thin disk at various black hole masses and Eddington ratios ( $\dot{m}$ ) overplotted with flux ratios and black hole masses for AGNs with measured  $M_{\text{BH}}$ . Model ratios were determined by multiplying a multicolor blackbody disk from XSPEC by the GALEX *FUV* and *NUV* bandpasses. Eddington ratios were calculated from the Grupe et al. bolometric luminosities, uncorrected for UV flux. Outliers (Tab. 6) are not shown. The accretion rates implied by these UV colors are significantly lower than the measured values, suggesting there must be a contribution from sources other than a standard thin disk. Error bars include statistical errors only.

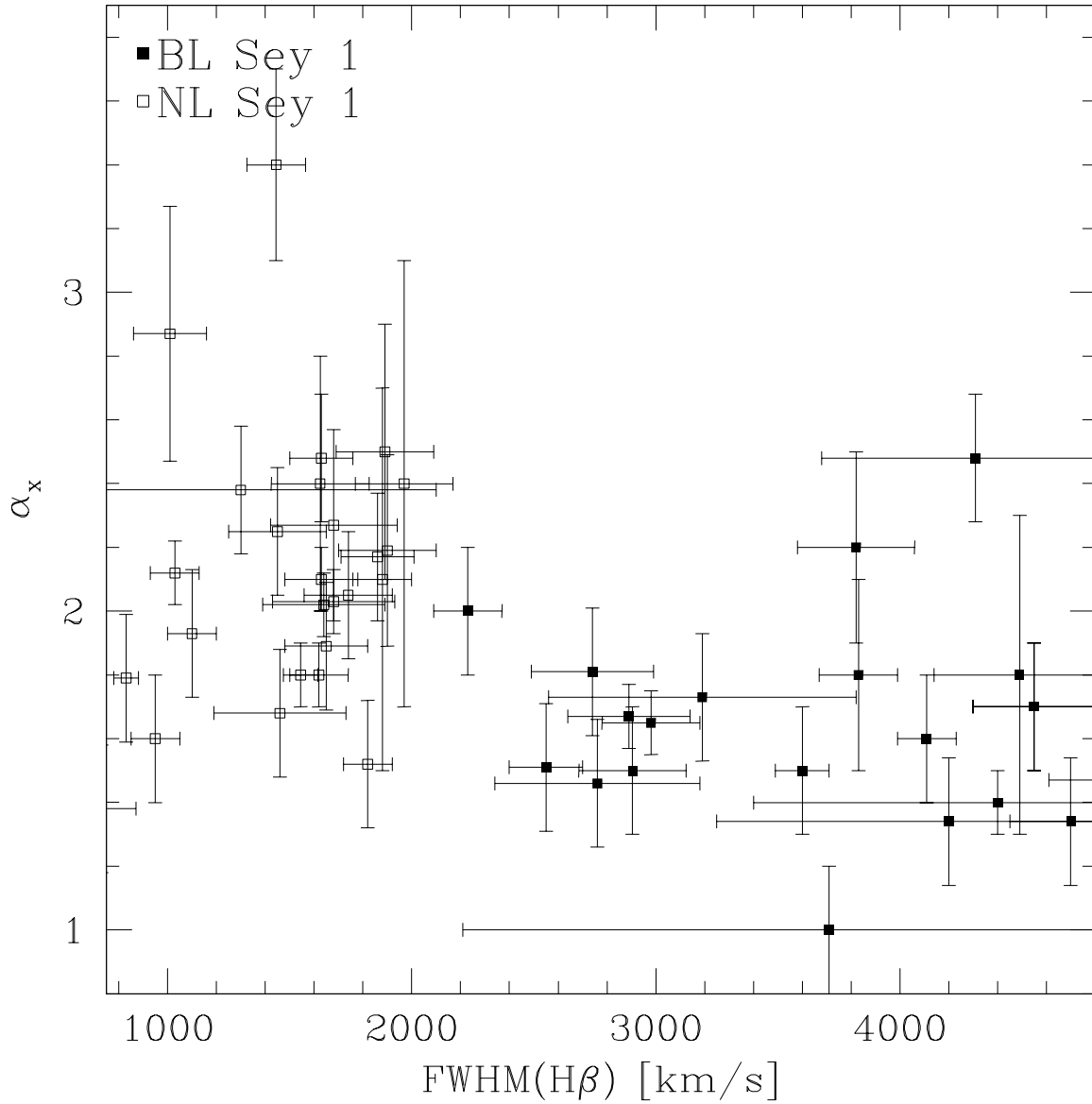


Fig. 11.— Relations between FWHM(H $\beta$ ) and the shape of the soft X-ray continuum. The Spearman test indicates a correlation between these parameters, but the data appear to be more consistent with the “zone of avoidance” reported by Boller, Brandt & Fink (1996).

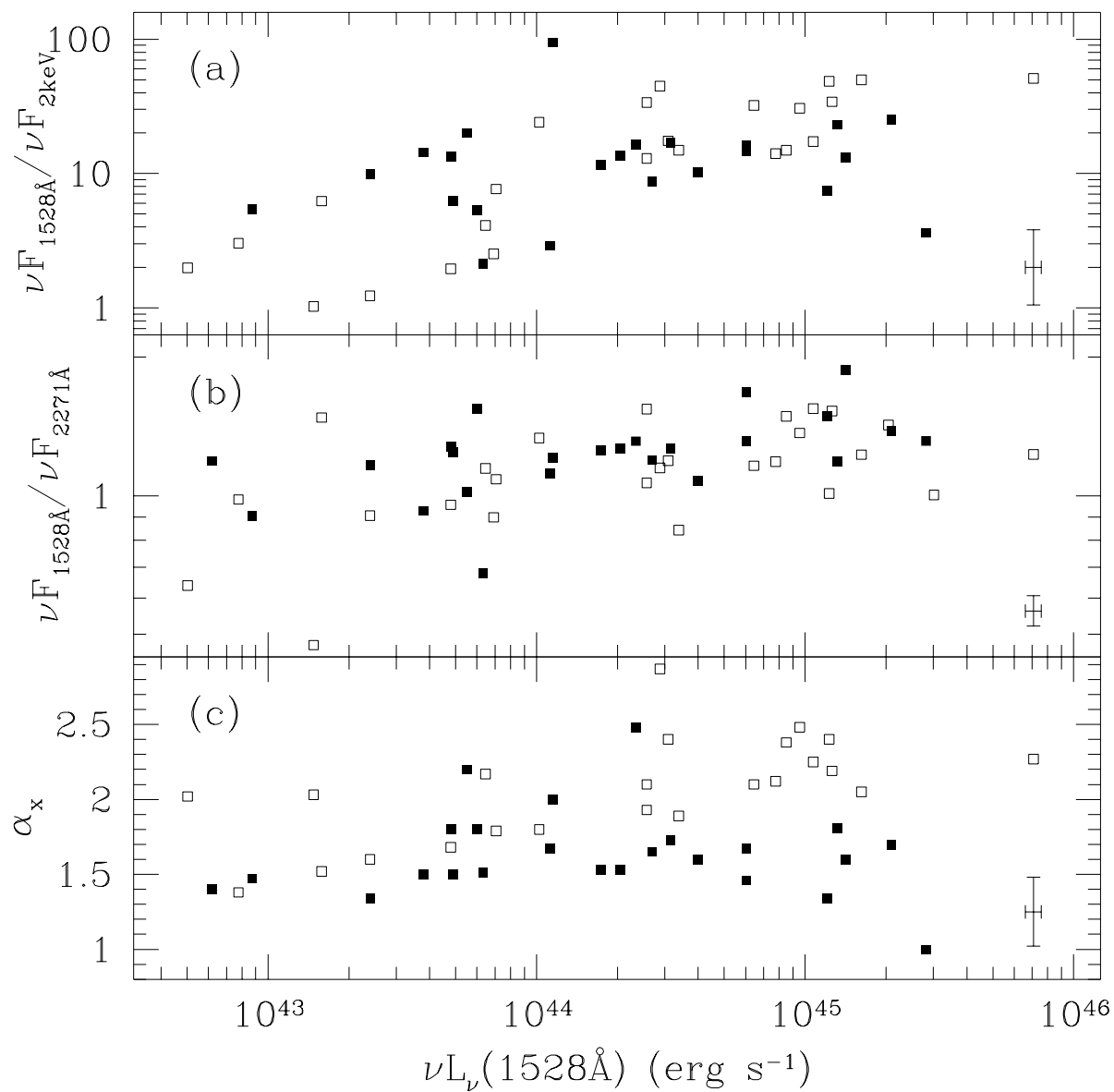


Fig. 12.— Relations between  $\nu L_\nu(1528 \text{ \AA})$  and various observable properties. The trends are obviously stronger among the NLS1 (*open*) sample than among the BLS1 (*filled*) sample. Error bars displayed on each panel represent the average uncertainties after excluding the outliers.

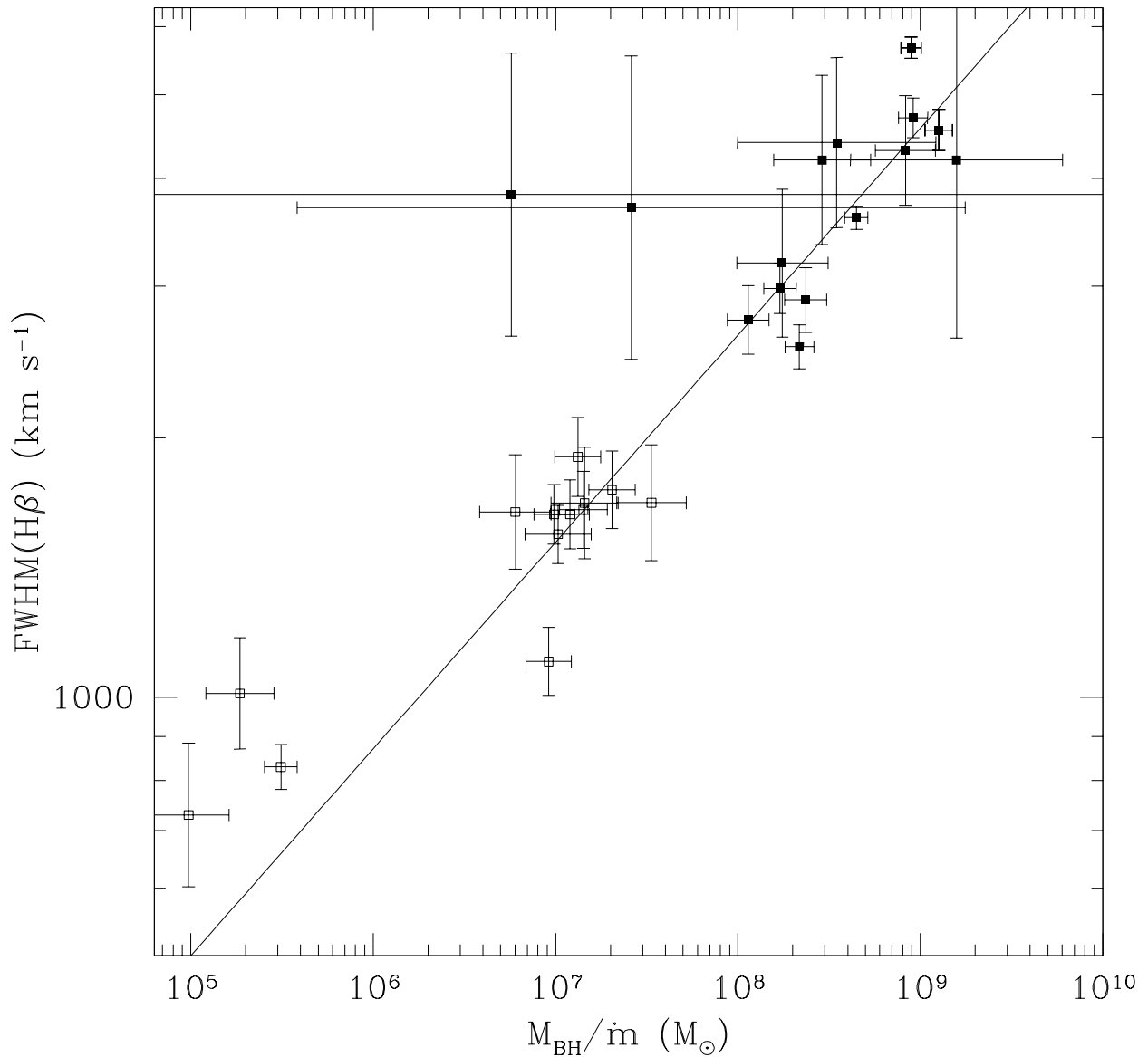


Fig. 13.— Line width as a function of the ratio between black hole mass ( $M_{BH}$ ) and Eddington ratio ( $\dot{m}$ ). Virial relationships predict  $w(\text{H}\beta) \propto (M_{BH}/\dot{m}_{\text{edd}})^{1/4}$ , assuming that  $R_{\text{BLR}} \propto L^{1/2}$ . Black hole masses were determined using the Kaspi et al. (2000) relation, and Eddington ratios were calculated from the bolometric luminosities listed in Grupe et al. (2004). The best fit relation to the full sample is  $\log[\text{FWHM}(\text{H}\beta)] = (0.24 \pm 0.02) \log[M_{BH}/(\dot{m}M_{\odot})] + (1.5 \pm 0.1)$ , which is consistent with a simple virialized structure for the broad line region. NLS1s are shown with *open* points and BLS1s with *filled* points.

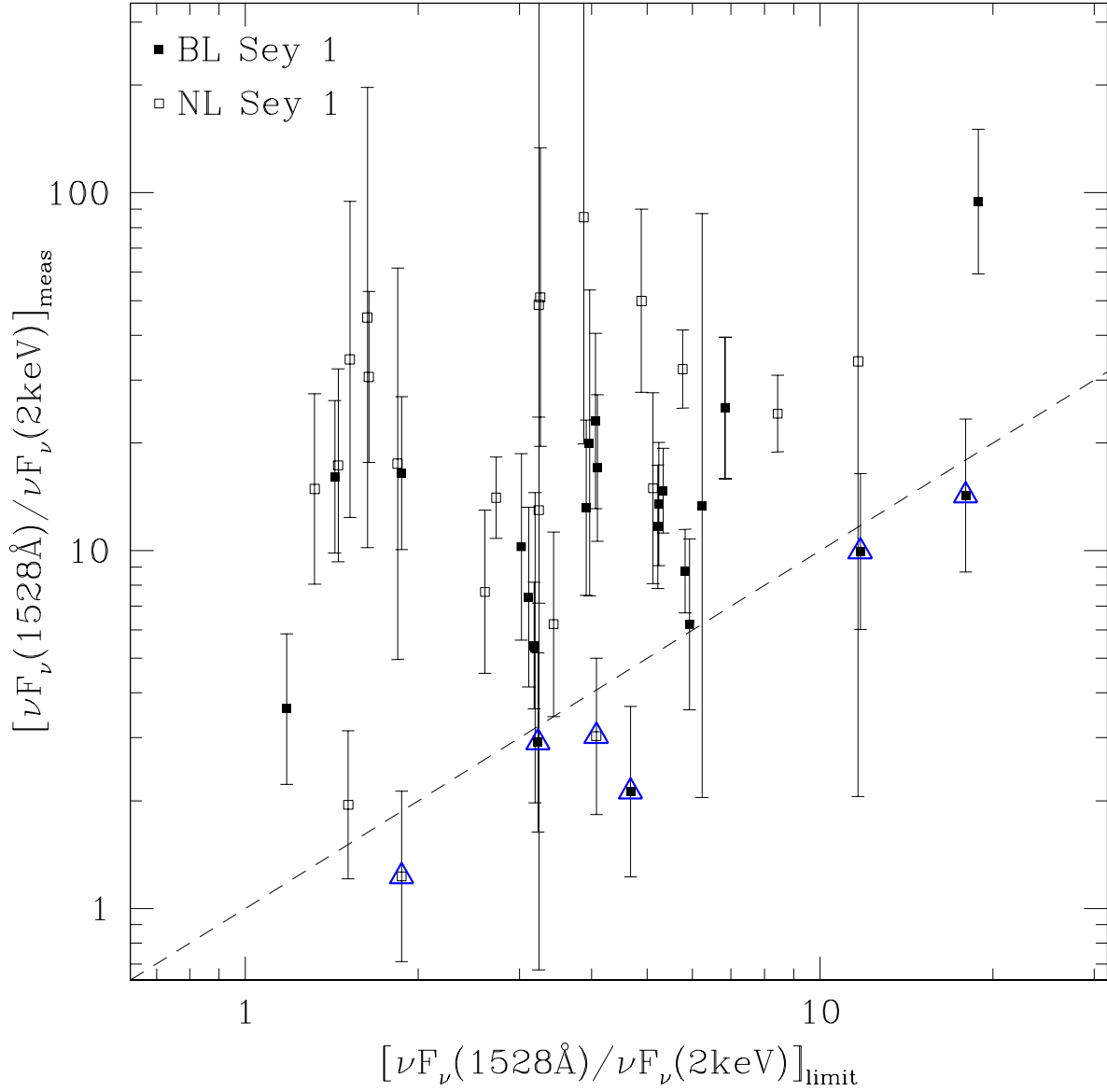


Fig. 14.— Comparison of  $\nu F_\nu(1528 \text{ \AA})/\nu F_\nu(2 \text{ keV})$  lower limits (x-axis) from our *ad hoc* model with the measured ratios (y-axis). The *dashed line* marks the line of equality, so any object to the right of the line (emphasized by the *blue triangles*) have lower limits in excess of the measured flux ratios.

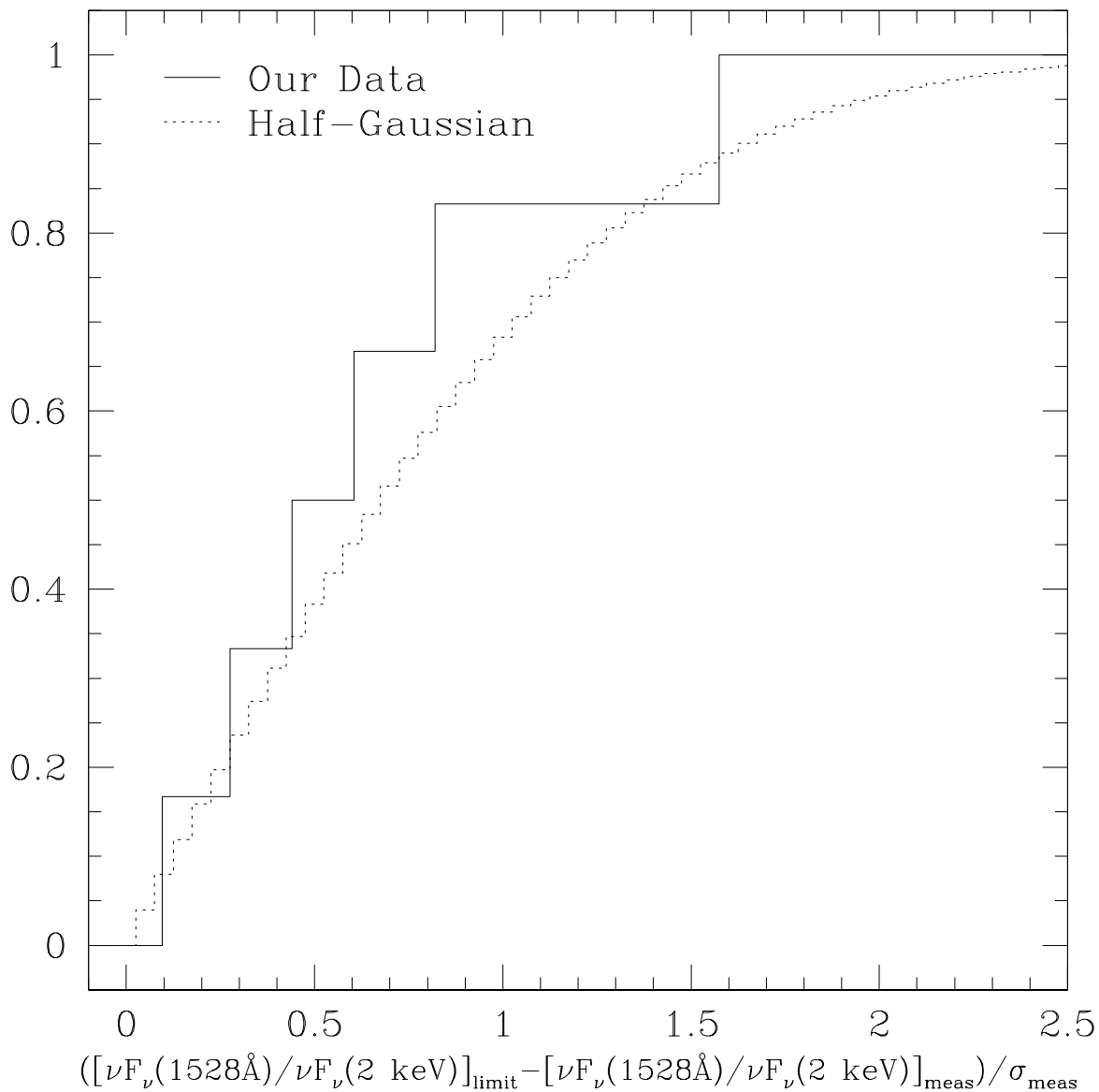


Fig. 15.— Cumulative distribution function of objects whose lower limits on  $\nu F_\nu(1528\text{ \AA})/\nu F_\nu(2\text{ keV})$  exceed the measured values (*solid*) compared with cumulative distribution of a half-Gaussian (*dotted*). The half-Gaussian has distribution function  $c(x) = \text{erf}(x/\sqrt{2})$ .